

AD-A102 161

NAVAL RESEARCH LAB WASHINGTON DC

F/6 4/2

FORMULATION OF A MODAL-SPLIT-EXPLICIT TIME INTEGRATION METHOD F--ETC(U)

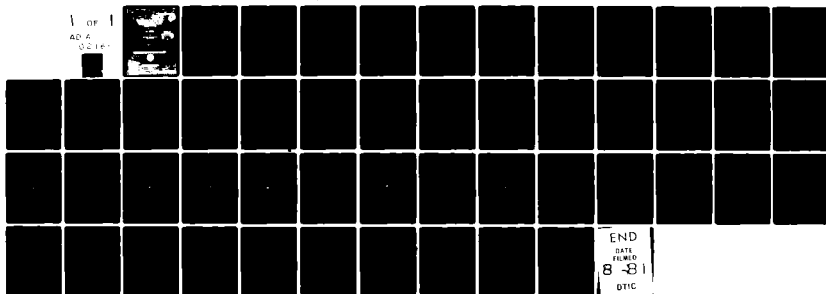
JUL 81 W C CHAO, R V MADALA

UNCLASSIFIED

NRL-MR-4572

NL

1 OF 1
AD-A
00161



END
DATE
FILMED
8-81
DTIC

AD A102161

SECURITY CLASSIFICATION OF THIS PAGE (When Data Entered)

REPORT DOCUMENTATION PAGE		READ INSTRUCTIONS BEFORE COMPLETING FORM
1. REPORT NUMBER NRL Memorandum Report 4572	2. GOVT ACCESSION NO. AD-A102 161	3. RECIPIENT'S CATALOG NUMBER
4. TITLE (and Subtitle) FORMULATION OF A MODAL-SPLIT-EXPLICIT TIME INTEGRATION METHOD FOR USE IN THE UCLA ATMOSPHERIC GENERAL CIRCULATION MODEL		5. TYPE OF REPORT & PERIOD COVERED Interim report on a continuing NRL problem.
7. AUTHOR(s) W.C. Chao and R.V. Madala		6. PERFORMING ORG. REPORT NUMBER
9. PERFORMING ORGANIZATION NAME AND ADDRESS Naval Research Laboratory Washington, D.C. 20375		8. CONTRACT OR GRANT NUMBER(s)
11. CONTROLLING OFFICE NAME AND ADDRESS Naval Environmental Prediction Research Facility Monterey, California 93940		10. PROGRAM ELEMENT PROJECT, TASK AREA & WORK UNIT NUMBERS 62759N; WR59-551; 47-0885-01
14. MONITORING AGENCY NAME & ADDRESS (if different from Controlling Office)		12. REPORT DATE July 24, 1981
		13. NUMBER OF PAGES 49
		15. SECURITY CLASS. (of this report) UNCLASSIFIED
		15a. DECLASSIFICATION/DOWNGRADING SCHEDULE
16. DISTRIBUTION STATEMENT (of this Report) Approved for public release; distribution unlimited.		
17. DISTRIBUTION STATEMENT (of the abstract entered in Block 20, if different from Report)		
18. SUPPLEMENTARY NOTES *Current address: Science Applications, Inc., McLean, Virginia 22102. This work was sponsored by the Naval Environmental Prediction Research Facility, Program Element 62759N, Project WR59-551, "Atmospheric Environmental Support."		
19. KEY WORDS (Continue on reverse side if necessary and identify by block number) General circulation model Numerical methods Weather prediction		
20. ABSTRACT (Continue on reverse side if necessary and identify by block number) With appropriate modifications, a recently proposed modal-split-explicit time integration scheme (MSES) is incorporated into the UCLA atmospheric general circulation model. In this scheme, the terms in the governing equations that generate the linear gravity waves are split into different vertical modes. Each mode is integrated with an optimal time step, and at periodic intervals these modes are recombined. The other terms are integrated with a time step dictated by the CFL condition for low frequency waves. This large time step requires a special modification of the advective terms in the polar region to maintain stability. Seventy-two hour test runs show that MSES is a viable, efficient, and accurate scheme for global weather prediction purposes.		

DD FORM 1473

EDITION OF 1 NOV 65 IS OBSOLETE
S/N 0102-014-6601

SECURITY CLASSIFICATION OF THIS PAGE (When Data Entered)

CONTENTS

1.0 INTRODUCTION	1
2.0 FORMULATION	3
2.1 Basic Equations	3
2.2 The Modal-Split-Explicit Method	6
2.3 Modification of the Advective Terms Near the Poles	13
2.4 The Time Differencing Method	15
2.5 Addition of the Pressure Averaging Method	15
3.0 RESULTS AND DISCUSSION	16
3.1 Stability	16
3.2 Efficiency	17
3.3 Accuracy	17
ACKNOWLEDGMENTS	20
APPENDIX	38
REFERENCES	43

Accession For	
NTIS GRA&I	<input checked="checked" type="checkbox"/>
DTIC TAB	<input type="checkbox"/>
Unannounced	<input type="checkbox"/>
Justification	
By _____	
Distribution/ _____	
Availability Codes	
Dist	Avail and/or Special
A	

FORMULATION OF A MODAL-SPLIT-EXPLICIT TIME INTEGRATION METHOD
FOR USE IN THE UCLA ATMOSPHERIC GENERAL CIRCULATION MODEL

1.0 INTRODUCTION

In the explicit time integration of primitive equations, the time step is limited by the Courant-Friedrichs-Lewy (CFL) condition (Courant et al., 1928), based on the fastest phase speed of waves allowed in the model, which is the speed of the external gravity wave; thus the integration is rather slow. Since the meteorologically significant waves have speeds much slower than that of the external gravity wave and possess practically all of the energy of the atmospheric motion, the use of the explicit scheme is rather uneconomical. Two major approaches have been taken to circumvent this difficulty. First, since the gravity waves are quasi-linear, the portion of the primitive equations that govern the linear gravity waves can be integrated implicitly, and the rest of the equations can be integrated explicitly with a time step dictated by the CFL condition for slow moving waves. Known as the semi-implicit method, it has been used both in grid point models (Kwizak and Robert, 1971) and in spectral models (Robert, 1969) with significant savings in computing time and acceptable accuracy (Robert, et al., 1972). However, since the speed of the gravity waves is reduced in the implicit integration, its accuracy is questionable in the regions of gravity waves excitation (Messinger and Arakawa, 1977). The semi-implicit method can be modified; the terms governing the linear gravity waves can be separated into different vertical modes. Only modes with phase speeds greater than those of the meteorological waves--usually the external gravity wave and the

first two or three internal gravity waves--need to be integrated implicitly (Burridge, 1978).

The second approach to expedite the integration involves separating the terms related to the gravity waves from the rest of the equations. One group of terms is integrated first with an optimal time step, either explicitly or implicitly, and the result of this step is used at the beginning of the marching for the other group, employing a different optimal time step. This is called the splitting method (Marchuk, 1974; Gadd, 1978). When explicit schemes are used, the splitting method does not have the adverse effect of retarding the gravity waves. However, since the different dynamic processes are calculated one at a time, the truncation errors of all steps are multiplied rather than added.

In a logical progression Madala (1980)* proposed a modal-split-explicit scheme (MSES), which combines the advantages of the aforementioned methods, yet avoids their shortcomings. In this method terms in the primitive equations governing linear gravity waves are decomposed into different vertical modes. Modes with phase speeds greater than the meteorological waves are integrated explicitly, with time steps allowed by the respective CFL conditions and are recombined at periodic intervals. The other modes and the rest of the equations are integrated explicitly with a time step determined by the speed of the slow moving waves, which is usually five times as large as the time step allowed for the fastest moving waves. This constitutes great savings in computing time. In addition since all waves

*Madala (1981) used the name "split-explicit;" the first author added the word "modal" to distinguish it from the split-explicit schemes used by other authors.

are integrated explicitly, no adverse effect on gravity wave speed occurs. Moreover, since all dynamic terms are integrated (or marched) simultaneously, the multiplicative truncation error characteristic of the splitting methods is avoided.

Thus far, MSES has been successfully applied to a tropical cyclone model (Madala, 1981). The speed of integration was increased by a factor of three over that using the explicit method; this factor, however, is an increasing function of horizontal resolution. The results also showed good accuracy. The present paper presents a further investigation of MSES in order to ascertain whether it is also a viable method in a global model, in which more complexities exist, such as high terrain and the diminishing zonal grid size toward the poles. The model chosen for this effort is the 1977 version of the UCLA model (Arakawa and Lamb, 1977; hereafter referred to as AL; Arakawa and Mintz, 1974).

This investigation shows that modifications are necessary (Section 2.2); that additional features should be added (Section 2.3); and that the pressure averaging technique can be used to improve the efficiency of MSES (Section 2.5). In addition, the results of a 72-hour test run showed that MSES is viable, efficient, and accurate for global weather prediction purposes.

2.0 FORMULATION

2.1 Basic Equations

Since MSES treats the terms governing linear gravity waves in the equations of motion differently from the rest, these terms must first be identified. The vertical coordinates

in the UCLA GCM is

$$\sigma \equiv \frac{P - P_T}{\pi}, \quad (1)$$

where P is pressure; P_T is a constant pressure at the model top (currently $P_T = 50$ mb); $\pi \equiv P_S - P_T$; and P_S is the pressure at the surface. Because there is only one layer in the stratosphere, the original definition of σ in the stratosphere (AL, p. 207) is not used for reasons of simplicity. All notations follow those of AL unless otherwise indicated.

The zonal momentum equation in the flux form is

$$\begin{aligned} \frac{\partial}{\partial t} (\pi u) + \frac{\partial}{\partial x} (\pi u^2) + \frac{1}{\cos^2 \phi} \frac{\partial}{\partial y} (\pi u v \cos^2 \phi) \\ + \frac{\partial}{\partial \sigma} (\pi u \dot{\sigma}) - \pi f v = -\pi \left(\frac{\partial \phi}{\partial x} \right)_{\sigma} \\ - (\pi \sigma \alpha) \left(\frac{\partial \pi}{\partial x} \right)_{\sigma} + \pi F_x, \end{aligned} \quad (2)$$

where u is zonal velocity, v , meridional velocity; ϕ , geopotential; α , specific volume; f , Coriolis parameter; ϕ , latitude, λ , longitude; a , earth's radius; F_x , zonal frictional force; $\dot{\sigma} = d\sigma/dt$; $\partial x = a \cos \phi \partial \lambda$; and $\partial y = a \partial \phi$.

Since $\phi = \phi_s + \phi_a$, where ϕ_s is the surface geopotential and ϕ_a is the ϕ measured from surface, the pressure gradient force terms in Eq. (2) can be written as

$$-\frac{\partial}{\partial x} (\pi \phi_a) + \left[\overline{(\phi_a - \sigma \pi \alpha)} + (\phi_a - \sigma \pi \alpha)' \right] \frac{\partial}{\partial x} \pi - \pi \frac{\partial}{\partial x} \phi_s,$$

where the double bar denotes global average on a σ -surface, and the prime denotes the deviation from it. If $\bar{\phi} \equiv \pi \phi_a -$

$\overline{(\phi_a - \sigma \pi \alpha)} \pi$, Eq. (2) becomes

$$\frac{\partial}{\partial t} (\pi u) + \frac{\partial}{\partial x} \bar{\bar{\phi}} = R_u, \quad (3)$$

where R_u denotes remaining terms, which vary slowly in time compared to the terms on the left side of Equation (3). The additional operator, denoted by the dash bar, suppresses the amplitude of the short waves to overcome the problem associated with the diminishing zonal grid size. This operator is fully described in AL, p. 248, and should be applied to the zonal pressure gradient term and to the zonal mass flux term. In a similar manner, the equation governing meridional momentum can be written as:

$$\frac{\partial}{\partial t} (\pi v) + \frac{\partial}{\partial y} \bar{\bar{\phi}} = R_v. \quad (4)$$

The surface pressure tendency equation is,

$$\frac{\partial}{\partial t} \pi + \langle N_2 \rangle^T \langle D \rangle = 0, \quad (5)$$

where $D \equiv \nabla \cdot (\pi v) = \frac{\partial}{\partial x} (\bar{\bar{\pi u}}) + \frac{1}{\cos \phi} \frac{\partial}{\partial y} (\pi v \cos \phi)$ (AL, Eq. (166)).

The row vector $\langle N_2 \rangle^T$ is given in the appendix.

The thermodynamic equation (AL, Eq. (209)) is

$$\begin{aligned} \frac{\partial}{\partial t} (\pi T_k) + \nabla \cdot (\pi v_k T_k) + \frac{1}{\Delta \sigma_k} \left[(\pi \hat{\sigma})_{k+\frac{1}{2}} p_k \hat{\theta}_{k+\frac{1}{2}} \right. \\ \left. - (\pi \hat{\sigma})_{k-\frac{1}{2}} p_k \hat{\theta}_{k-\frac{1}{2}} \right] = \frac{1}{C_p} (\sigma \pi \alpha)_k \left(\frac{\partial}{\partial t} + v_k \cdot \nabla \right) \pi + \frac{\pi}{C_p} Q_k, \end{aligned} \quad (6)$$

where the subscripts are level indices; θ , potential temperature;
 $p \equiv T/\theta \equiv \left(\frac{P}{1000}\right)^K$; and C_p , specific heat at constant pressure.

Integration of the continuity equation gives $\langle \pi \dot{0} \rangle = [N_1] \langle D \rangle$.

Thus, Eq. (6) can be written as:

$$\frac{\partial}{\partial t} (\pi T_k) + \overline{T_k} D_k + \frac{1}{C_p} (\sigma \pi \alpha)_k \langle N_2 \rangle^T \langle D \rangle$$

$$+ ([M_4] \langle D \rangle)_k = \langle R_{T_k} \rangle ,$$

or as:

$$\frac{\partial}{\partial t} (\pi \langle T \rangle) + [M_2] \langle D \rangle = \langle R_T \rangle , \quad (7)$$

where $[M_4] \langle D \rangle$ denotes the linear part of the last two terms on the left side of Equation (6), and R_T denotes all the remaining terms. The matrices $[M_2]$ and $[M_4]$ are given in the appendix. Instead of π , $\bar{\pi}$ is used in computing $[M_4]$.

Equations (3), (4), (5), (6) and the hydrostatic equation form the complete set of governing equations in the model. When $R_u = R_v = R_T = 0$, these equations govern the linear gravity waves in an atmosphere with no basic motion.

2.2 The Modal-Split-Explicit Method

In the UCLA GCM, ϕ_a is related to the temperature nonlinearly (AL, Eqs. (207)-(208)), and this will be denoted by a subscript N, thus $(\phi_a)_N$. However, one important requirement in the present scheme is that ϕ_a must be linearly related to temperature. This requirement is met by a previous definition of ϕ_a in the UCLA model (Arakawa, 1972; and Appendix), and this will be denoted by a subscript L, thus $(\phi_a)_L$. Accordingly, the

hydrostatic equation has the form: $\langle \phi_a \rangle_L = [M_1] \langle T \rangle$, where $[M_1]$ is given in the appendix. The matrix $[M_1]$ is a function of π , when P_T in Eq. (1) is not equal to zero; therefore, it is a function of the horizontal coordinates. As part of the simplification, $[M_1]$ computed with $\bar{\pi}$ will be used for all locations. In this way, the definition of $\langle \phi_a \rangle_L$ is modified.

Following the incorporation of the foregoing arguments Equation (3) should be rewritten as:

$$\frac{\partial}{\partial t} (\pi u) + \frac{\partial}{\partial x} \bar{\bar{\bar{\phi}}}_N = R_u. \quad (8)$$

When using leapfrog scheme in time, the finite difference form of (3) over a $2\Delta\tau$ interval can be written as,

$$\begin{aligned} (\pi u)^{t-\Delta t+(n+1)\Delta\tau} - (\pi u)^{t-\Delta t+(n-1)\Delta\tau} + 2\Delta\tau \frac{\partial}{\partial x} \bar{\bar{\bar{\phi}}}_N^{t-\Delta t+n\Delta\tau} \\ = 2\Delta\tau R_u^{t-\Delta t+n\Delta\tau}, \end{aligned} \quad (9)$$

where $\Delta\tau$ is a time interval allowed by the CFL condition based on the speed of fastest waves, and Δt is that based on the meteorological waves. The subscript N indicates that it is computed using nonlinear form of hydrostatic equation. Marching Eq. (9) with $2\Delta\tau$ intervals between $t-\Delta t$ and $t+\Delta t$ and averaging these equations in time given,

$$\begin{aligned} (\pi u)^{t+\Delta t} - (\pi u)^{t-\Delta t} + 2\Delta t \frac{\partial}{\partial x} \bar{\bar{\bar{\phi}}}_N^{t-2\Delta t} \\ = 2\Delta t \bar{R}_u^{2\Delta t} \doteq 2\Delta t R_u^t, \end{aligned} \quad (10)$$

where $(\bar{\cdot})^{2\Delta t}$ is the discrete averaging over the $2\Delta t$ interval. With regard to the stability of the scheme, the approximation of $\bar{R}_u^{2\Delta t}$ by R_u^t is allowed, since R_u does not create a high frequency variation in πu , and since it is a slow varying term. This approximation introduces a truncation error, which is, however, bearable. When the term $2\Delta t \frac{\partial}{\partial x} \left(\bar{\frac{\pi}{\phi_L}}^{2\Delta t} - \bar{\frac{\pi}{\phi_N}}^{2\Delta t} + \bar{\frac{\pi}{\phi_L}}^t \right)$ is added to both sides, Eq. (10) becomes

$$\begin{aligned}
 (\pi u)^{t+\Delta t} - (\pi u)^{t-\Delta t} + 2\Delta t \frac{\partial}{\partial x} \left(\bar{\frac{\pi}{\phi_L}}^{2\Delta t} - \bar{\frac{\pi}{\phi_L}}^t \right) \\
 &= 2\Delta t R_u^t + 2\Delta t \frac{\partial}{\partial x} \left(\bar{\frac{\pi}{\phi_L}}^{2\Delta t} - \bar{\frac{\pi}{\phi_N}}^{2\Delta t} - \bar{\frac{\pi}{\phi_L}}^t \right) \\
 &\doteq 2\Delta t R_u^t + 2\Delta t \frac{\partial}{\partial x} \left(\bar{\frac{\pi}{\phi_L}}^t - \bar{\frac{\pi}{\phi_N}}^t - \bar{\frac{\pi}{\phi_L}}^t \right) \\
 &= 2\Delta t R_u^t - 2\Delta t \frac{\partial}{\partial x} \bar{\frac{\pi}{\phi_N}}^t .
 \end{aligned} \tag{11}$$

The right side of Eq. (11) gives the change of πu over the $2\Delta t$ interval in one leapfrog step. Therefore, Eq. (11) becomes:

$$\begin{aligned}
 (\pi u)^{t+\Delta t} - (\pi u)^{t-\Delta t} + 2\Delta t \frac{\partial}{\partial x} \left(\bar{\frac{\pi}{\phi_L}}^{2\Delta t} - \bar{\frac{\pi}{\phi_L}}^t \right) \\
 &= (\pi u)_E^{t+\Delta t} - (\pi u)^{t-\Delta t} ,
 \end{aligned} \tag{12}$$

where the subscript E denotes the results from marching once with the $2\Delta t$ interval without the help of the MSES scheme. Thus, $(\pi u)^{t+\Delta t}$ can be found by marching Eq. (8) over $2\Delta t$ only once, if $\bar{\phi_L}^{2\Delta t}$ is known.

Similarly, the other governing equations are:

$$\begin{aligned}
 (\pi v)^{t+\Delta t} - (\pi v)^{t-\Delta t} + 2\Delta t \frac{\partial}{\partial y} (\tilde{\phi}_L^{2\Delta t} - \bar{\phi}_L^t) \\
 = (\pi v)_E^{t+\Delta t} - (\pi v)^{t-\Delta t} ,
 \end{aligned} \tag{13}$$

$$\begin{aligned}
 \langle \pi T \rangle^{t+\Delta t} - \langle \pi T \rangle^{t-\Delta t} + 2\Delta t [M_2] \langle \tilde{D}^{2\Delta t} - D^t \rangle \\
 = \langle \pi T \rangle_E^{t+\Delta t} - \langle \pi T \rangle^{t-\Delta t} ,
 \end{aligned} \tag{14}$$

and

$$\begin{aligned}
 \pi^{t+\Delta t} - \pi^{t-\Delta t} + 2\Delta t \langle N_2 \rangle^T \langle \tilde{D}^{2\Delta t} - D^t \rangle \\
 = \pi_E^{t+\Delta t} - \pi^{t-\Delta t} .
 \end{aligned} \tag{15}$$

Since the aim now is to obtain the two sets of unknowns, $\langle \tilde{\phi} \rangle^{2\Delta t}$ and $\langle \tilde{D} \rangle^{2\Delta t}$, the four sets of equations can be reduced to two sets. Forming $[M_1](14) + \langle \overline{\sigma\pi\alpha - \phi_L} \rangle (15)$ gives:

$$\begin{aligned}
 \langle \bar{\phi} \rangle^{t+\Delta t} - \langle \bar{\phi} \rangle^{t-\Delta t} + 2\Delta t [M_3] \langle \tilde{D}^{2\Delta t} - D^t \rangle \\
 = \langle \bar{\phi} \rangle_E^{t+\Delta t} - \langle \bar{\phi} \rangle^{t-\Delta t} ,
 \end{aligned} \tag{16}$$

where $[M_3] = [M_1] [M_2] + \overline{\langle \sigma \pi \alpha - \phi_L \rangle} \langle N_2 \rangle^T$. The grid scheme C (AL, p. 182) used in the UCLA model is not changed.

In order to form the divergence equation from Eqs. (12) and (13) it is convenient to define π at the $u(v)$ points as the average of the two neighboring π 's in the zonal (meridional) direction. However, it should be emphasized that the original definition of π at the u and v points (AL, p. 242) are still used in computing $u_E^{t+\Delta t}$ and $v_E^{t+\Delta t}$.

Equations (12) and (13) give the divergence equation

$$\begin{aligned} \langle D \rangle^{t+\Delta t} - \langle D \rangle^{t-\Delta t} + 2\Delta t \nabla^2 \langle \frac{\bar{\phi}}{L} 2\Delta t - \frac{\bar{\phi}}{L} t \rangle \\ = \langle D \rangle_E^{t-\Delta t} - \langle D \rangle^{t-\Delta t}, \end{aligned} \quad (17)$$

where $\nabla^2 = \frac{\partial^2}{\partial x^2} + \frac{1}{\cos \phi} \frac{\partial}{\partial y} \left(\cos \phi \frac{\partial}{\partial y} \right)$. Note that the dash bar operator is used twice. Spectral equations governing the amplitudes of the natural gravity modes of the numerical model can be obtained by premultiplying equations (16) and (17) by $[E]^{-1}$, where $[E]$ is a matrix whose columns are the eigenvectors of $[M_3]$.

The spectral equations are,

$$\begin{aligned}
& \left(\langle \bar{\phi}_L^E \rangle^{t+\Delta t} - \langle \bar{\phi}_L^E \rangle^t \right) - \left(\langle \bar{\phi}_L^E \rangle^{t-\Delta t} - \langle \bar{\phi}_L^E \rangle^t \right) \\
& + 2\Delta t [\lambda] \langle \bar{D}^E \rangle^{2\Delta t} - \langle \bar{D}^E \rangle^t > \\
& = [E]^{-1} \left(\langle \bar{\phi}_L^E \rangle_E^{t+\Delta t} - \langle \bar{\phi}_L^E \rangle^{t-\Delta t} \right) , \quad (18)
\end{aligned}$$

and

$$\begin{aligned}
& \left(\langle D^E \rangle^{t+\Delta t} - \langle D^E \rangle^t \right) - \left(\langle D^E \rangle^{t-\Delta t} - \langle D^E \rangle^t \right) \\
& + 2\Delta t \nabla^2 \langle \bar{\phi}_L^E \rangle^{2\Delta t} - \langle \bar{\phi}_L^E \rangle^t > \\
& = [E]^{-1} \left(\langle D^E \rangle_E^{t+\Delta t} - \langle D^E \rangle^{t-\Delta t} \right) , \quad (19)
\end{aligned}$$

where $[\lambda]$ is equal to $[E]^{-1}[M_3][E]$, a diagonal matrix whose diagonal elements are the eigenvalues of $[M_3]$ and $\langle x \rangle^E \equiv [E]^{-1} \langle x \rangle$. Equations (18) and (19) can be used in a $\Delta\tau$ interval, and thus are written as:

$$\begin{aligned}
& \left(\langle \bar{\phi}_L^E \rangle^{\tau+\Delta\tau} - \langle \bar{\phi}_L^E \rangle^\tau \right) - \left(\langle \bar{\phi}_L^E \rangle^{\tau-\Delta\tau} - \langle \bar{\phi}_L^E \rangle^\tau \right) \\
& + 2\Delta\tau [\lambda] \langle \bar{D}^E \rangle^{\tau} - \langle \bar{D}^E \rangle^t > \\
& = \left(\Delta\tau / \Delta t \right) [E]^{-1} \left(\langle \bar{\phi}_L^E \rangle_E^{\tau+\Delta\tau} - \langle \bar{\phi}_L^E \rangle^{\tau-\Delta\tau} \right) \quad (20)
\end{aligned}$$

and

$$\begin{aligned}
 & \left(\langle D^E \rangle^{\tau+\Delta\tau} - \langle D^E \rangle^t \right) - \left(\langle D^E \rangle^{\tau-\Delta\tau} - \langle D^E \rangle^t \right) \\
 & + 2\Delta\tau \nabla^2 \langle \bar{\phi}_L^E{}^\tau - \bar{\phi}_L^E{}^t \rangle \\
 & = \left(\Delta\tau / \Delta t \right) [E]^{-1} \left(\langle D^E \rangle^{t+\Delta t} - \langle D^E \rangle^{t-\Delta t} \right), \quad (21)
 \end{aligned}$$

where the right sides of these equations are not changed (except for the $\Delta\tau/\Delta t$ factor), since they vary rather slowly over a $2\Delta t$ period.

Equations (20) and (21) are marched in the $2\Delta t$ interval with different $\Delta\tau$ for each mode as determined by the CFL condition based on the phase speed of that mode. The right sides of Eqs. (19) and (20) are, of course, held constant in this marching. The quantities $(D^{\bar{E}^{2\Delta t}} - D^{E^t})$ and $(\bar{\phi}_L^{E^{2\Delta t}} - \bar{\phi}_L^{E^t})$ are obtained from averaging the results of this marching. Only modes with phase speeds greater than the maximum speed of the meteorological waves have to be marched in this manner. Finally E is multiplied with $(D^{\bar{E}^{2\Delta t}} - D^{E^t})$ and $(\bar{\phi}_L^{E^{2\Delta t}} - \bar{\phi}_L^{E^t})$ to obtain $(D^{\bar{E}^{2\Delta t}} - D^t)$ and $(\bar{\phi}_L^{E^{2\Delta t}} - \bar{\phi}_L^t)$ respectively.

In summary, the procedure of the MSES method is:

- (1) Calculate the matrices, and the eigenvalues and eigenvectors of $[M_3]$, using the pre-determined global mean quantities. This step is done only once,

- (2) Compute $\left(\langle \bar{\phi}_L^E \rangle^{t-\Delta t} - \langle \bar{\phi}_L^E \rangle^t \right)$ and $\left(\langle D^E \rangle^{t-\Delta t} - \langle D^E \rangle^t \right)$.
- (3) Use the larger time interval Δt , march forward one step and compute the right hand sides of Eqs. (20) and (21).
- (4) March Eqs. (20) and (21) with different $\Delta \tau$ for different modes. For the six-level UCLA model (AL, p. 176), only the first three modes need to be integrated with $\Delta \tau = (1/5, 1/3, 1/2)\Delta t$.
- (5) Average the result from step (4) to obtain $\left(\langle \bar{\phi}_L^E \rangle^{2\Delta t} - \langle \bar{\phi}_L^E \rangle^t \right)$ and $\left(\langle D^E \rangle^{2\Delta t} - \langle D^E \rangle^t \right)$ which then allow the calculation of the predicted quantities at $t+\Delta t$ in Eqs. (12) through (15).

Although the above descriptions are based on the leapfrog scheme, the changes are minor when using the Matsuno scheme, which is periodically used in the UCLA GCM, (AL, p. 260). In the first part of the Matsuno scheme, the superscripts $t+\Delta t$, $t-\Delta t$ and $2\Delta t$ in the above equations are changed to t^* , t and Δt , respectively. Then, in the second part of the Matsuno scheme, the superscripts $t-\Delta t$ and $2\Delta t$ are changed to t^* and Δt , respectively. In both parts, of course, the factor $2\Delta t$ is changed to Δt .

2.3 Modification of the Advective Terms Near the Poles

Even when Δt is increased by a factor of five, the dash bar operator, described in subsection 2.2, is sufficient to circumvent the problem of linear instability related to the gravity wave terms, due to the diminishing zonal grid

toward the poles. However, the advective terms $\partial/\partial x [(\overline{\pi u})q]$ --where q denotes u , v and T --can create linear instability near the poles when Δt is enlarged. The time increment allowed for the advective terms, Δt , is limited by $\Delta t < \epsilon \Delta x / (u + c_m)$, where c_m is the speed of the meteorological waves, u is that of the basic flow, and ϵ has a magnitude of the order of 1, with its exact value depending on the time differencing scheme used. When u is large in the polar region, where Δx is small, Δt cannot be increased by a factor of five. One obvious, yet undesirable, solution is to use a smaller Δt . The solution used here is to apply the dash bar operator to q in the terms $\partial/\partial x [(\overline{\pi u})q]$ in Eqs. (272) and (299) of AL. Thus, in step 2 of the MSES procedure in subsection 2.2, the second term in Eq. (299) is changed to (with notation of AL):

$$\delta_\xi [\overline{F(\overline{T})}]^\xi.$$

Also, the changes in Eq. (272) are to substitute Eq. (275) into Eq. (272) and then to apply the dash bar operator on u in those terms containing $\overline{F^*}$. Similar changes are made for the v component equation. Short-term tests (72 hrs.) show this method is successful in controlling linear instability; however, since the quadratic conservation properties no longer hold, there can be some side effects in this approach, as will be shown in the result section.

2.4 The Time Differencing Method

As shown in Figure 1, the time differencing method used to calculate the dynamic terms consists of a series of the leapfrog schemes, with a periodic insertion of the Matsuno scheme. The source and sink terms, and the vertical flux convergence term of the moisture equation, are calculated as an instantaneous adjustment. For $\Delta t = 30$ min., these calculations are done after each leapfrog or Matsuno step. Thus, the time differencing method for the physical processes is not changed.

2.5 Addition of the Pressure Averaging Method

The pressure averaging method (Shuman et al., 1972) can be applied to the integration of Eqs. (19) and (20) to reduce the overhead in using the MSES scheme. Briefly, when this method is used on the 2-D linear gravity wave equations,

$$\phi_t + gH u_x = 0 ,$$

and

$$u_t + \phi_x = 0 ,$$

where u is the perturbed wind in the x -direction, ϕ the perturbed geopotential of the free surface, and H the basic state surface height. The time differencing scheme has the form:

$$(\phi^{\tau+1} - \phi^{\tau-1})/2\Delta t + gH u_x = 0 ,$$

and

$$(u^{\tau+1} - u^{\tau-1})/2\Delta t + \hat{\phi}_x^{\tau} = 0 ,$$

where

$$(\hat{\phi})^{\tau} = \alpha [(\phi)^{\tau+1} + (\phi)^{\tau-1}] + (1-2\alpha) (\phi)^{\tau} .$$

with this method, Δt can be almost twice as large as that allowed by the CFL condition. Thus, when this method is applied to Eqs. (20) and (21) the term $\bar{\phi}^E$ is changed to $\hat{\phi}^E$. In the present investigation, $\alpha = 0.24$ is used. Thus, Eqs. (20) and (21) can be integrated with $\Delta \tau = (1/3, 1/2, 1/1.5)\Delta t$ for the first three modes. A detailed analysis of this method was performed by Brown and Campana (1978).

3.0 RESULTS AND DISCUSSION

The performance of the present MSES formulation is of course judged by its stability, efficiency, and accuracy. The following discussions are directed toward these characteristics.

3.1 Stability

Two 12-hr. and one 72-hr. runs starting from different initial conditions showed that the present MSES formulation is capable of avoiding linear instability. Since the linear stability criterion depends not only on

the wave speeds but also on the wind speed, present formulation should be tested with large wind speed, especially in the polar region where zonal grid size is small. In one preliminary 12-hr. test run the wind speed near the northpole reached more than 50m/s and no linear instability occurred.

3.2 Efficiency

Tests show that when the UCLA GCM with $\Delta\phi = 4^\circ$, $\Delta\lambda = 5^\circ$ and $\Delta t = 30$ min. (five times of the original Δt) was run on a CDC 175 without physical processes, the reduction in integration CPU time by MSES is 48% of which 4% is due to the addition of the pressure averaging methods. The efficiency can be greater if the resolution increases. The net reduction in CPU time for the full model depends on the amount of the CPU time used for the physical processes, which of course get no improvement from MSES. The reduction is 24% for the full UCLA GCM with the aforementioned grid size. Only when a large portion of CPU time is allocated to dynamic processes does it pay to adopt the MSES.

3.3 Accuracy

Two 72-hr. runs with and without MSES were made starting from the same well-balanced initial conditions, which is the end of another 72-hr. run. The initial conditions and the results at hour 72 are shown in Figures 2 and 3 for sea level pressure and 500 mb geopotential height, respectively. The difference between the two runs is very small when compared with the changes over 72 hrs. The RMS differences in surface pressure, in 500 mb geopotential height, and in 500 mb zonal wind

between the two runs are given in Table 1. The RMS difference in 500 mb geopotential height at hour 72 is 16 meters, which is very small, when compared with a typical forecast error of 75 meters. Also the RMS difference in 500 mb zonal wind at hour 72 is 2.4 m/s compared with the typical 48 hr. forecast error of 8.5 m/s. Although there was concern whether computing the matrices using a globally averaged π was appropriate for high terrain areas, no adverse effect over these regions was detected. One obvious discrepancy between the two runs is that after 72 hrs., a strong high centered at 35° E, 80° S, appeared in the run using MSES, whereas only a weak high occupied this region in the other run. A separate 72-hr. run using MSES, and starting from the same initial conditions but without the physical processes, also has this intense high (Figure 4). Thus, it is reasonable to consider this discrepancy a side effect of the modification described in Section 2.3.

Table 1. RMS Differences

	RMS Difference		
	Surface Pressure (mb)	500 mb Geopotential Height (m)	500 mb Zonal Wind (m/s)
24 hr.	1.09	8.93	1.03
48 hr.	1.54	12.40	1.79
72 hr.	1.97	15.78	2.40

Overall, the results are remarkably good outside the regions very close to the poles. The poor performance near the poles, however, is not a direct consequence of applying MSES, but it is related to the horizontal differencing scheme, and to the diminishing zonal grid size near the poles. Whether this problem precludes long-term integration was not answered in this study, due to the limitations on computing resources.

Thus far the discussion on accuracy is based on the runs starting from a well-balanced initial condition. Whether the good accuracy can still be maintained in runs starting from an initial condition that is generated from an initialization program is again not answered due to the limitations on computing resources. Nevertheless, since a reasonably good initialization program should generate a fairly balanced initial condition, this problem may not be a justified concern. (However, incompatibility between the initial thermodynamic fields and the cumulus parameterization scheme can generate initial imbalance.) Besides, should this problem be serious, the use of MSES can be delayed for a while (say, 12 hrs.), after the initial imbalance has died down.

ACKNOWLEDGMENTS

This work was funded by the Naval Environmental Prediction Research Facility Program Element 62759N, Project WR59-551, "Atmospheric Environmental Support". Dr. Thomas E. Rosmond of Naval Environmental Prediction Research Facility provided the initial conditions for the test runs. His help in making the computing facility at Naval Fleet Numerical Oceanography Center accessible is greatly appreciated. Thanks are also extended to Drs. Simon W. Chang, Kay E. Cheney, and Darrell Strobel for reading the manuscript.

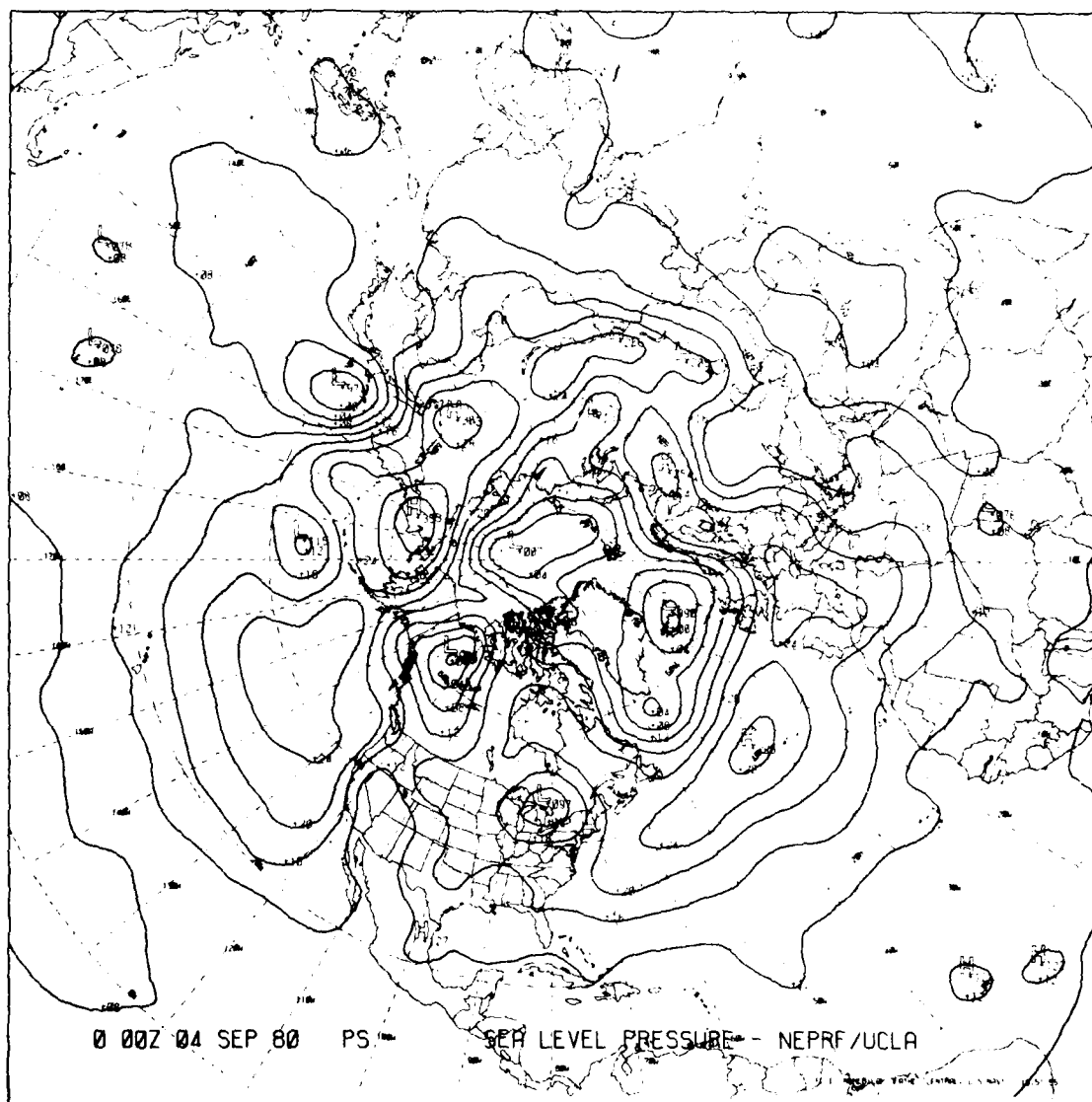


Fig. 2a — Initial sea level pressure (mb), Northern Hemisphere

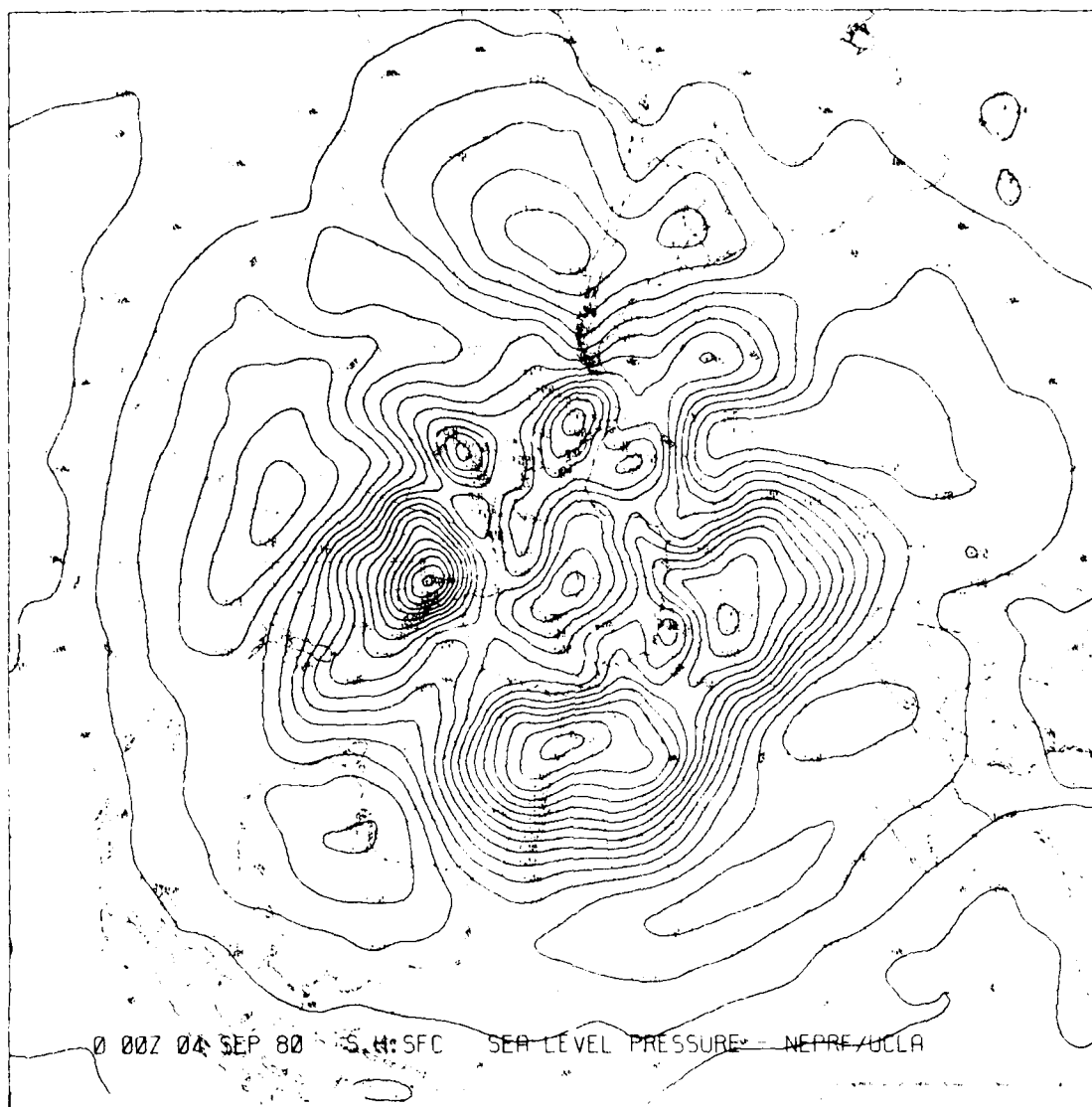


Fig. 2b — Initial sea level pressure (mb), Southern Hemisphere

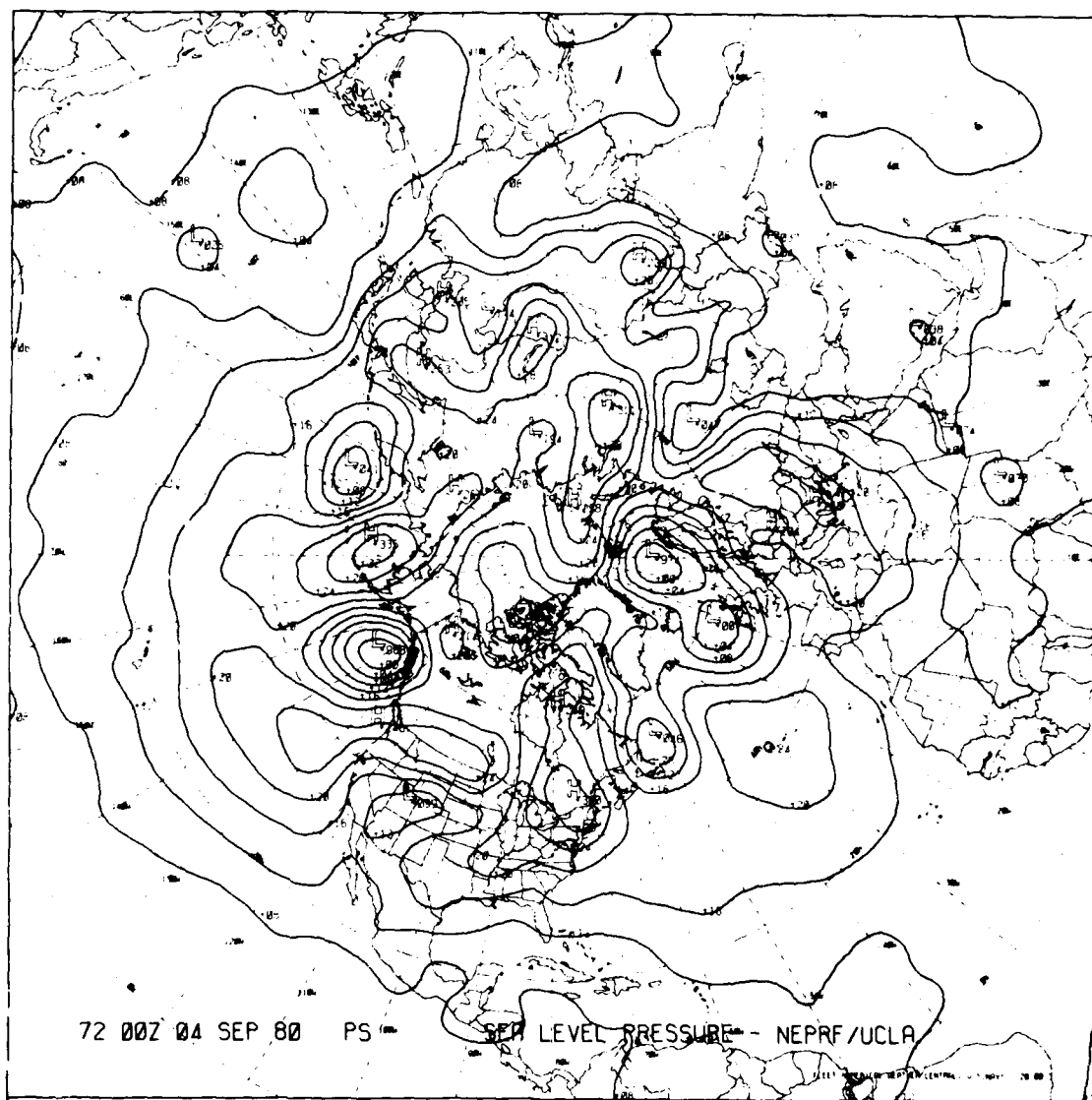


Fig. 2c — 72 hr. sea level pressure (mb), Northern Hemisphere, no MSES

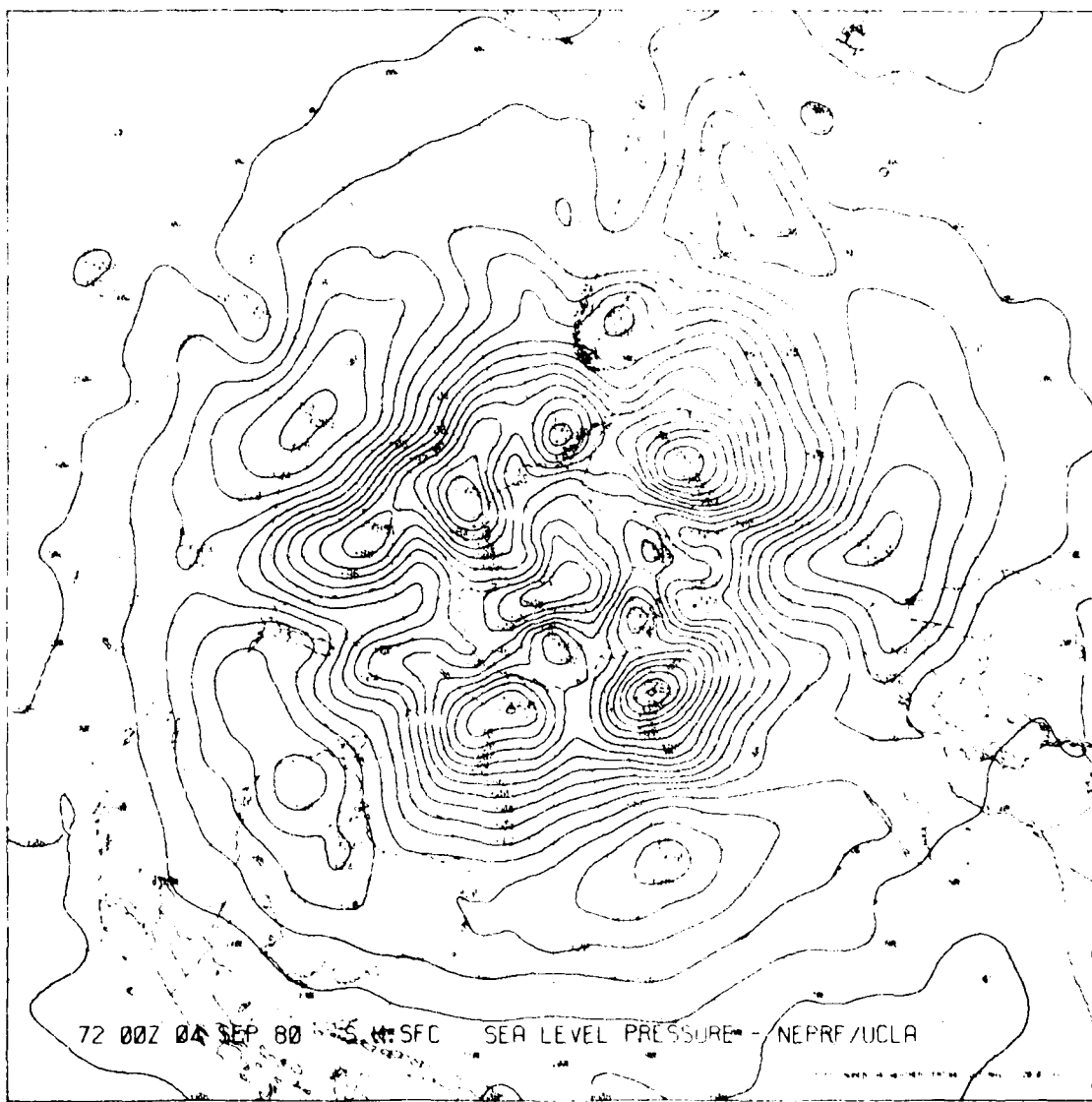


Fig. 2d — 72 hr. sea level pressure (mb), Southern Hemisphere, no MSES

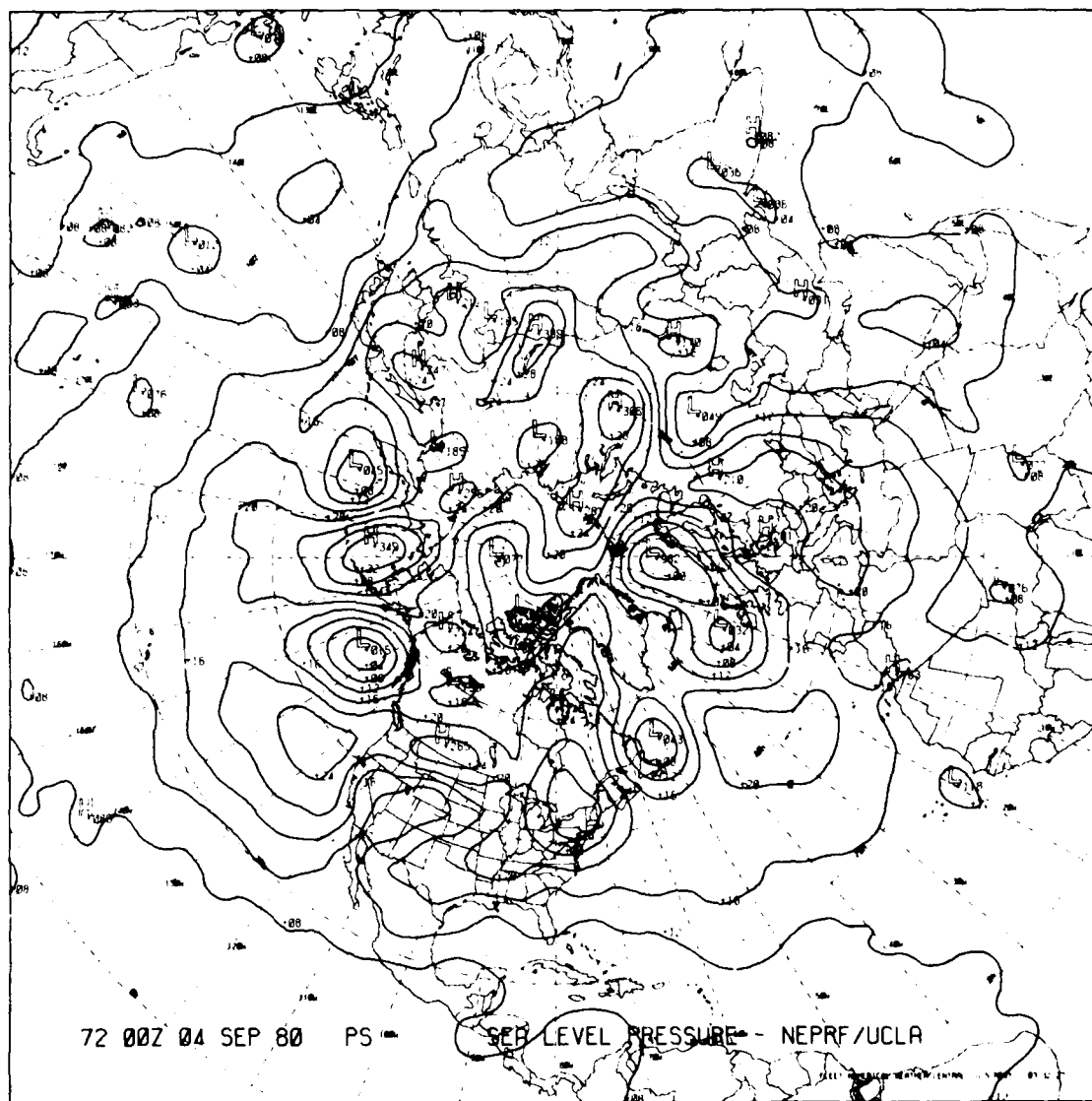


Fig. 2e — 72 hr. sea level pressure (mb), Northern Hemisphere, with MSEs

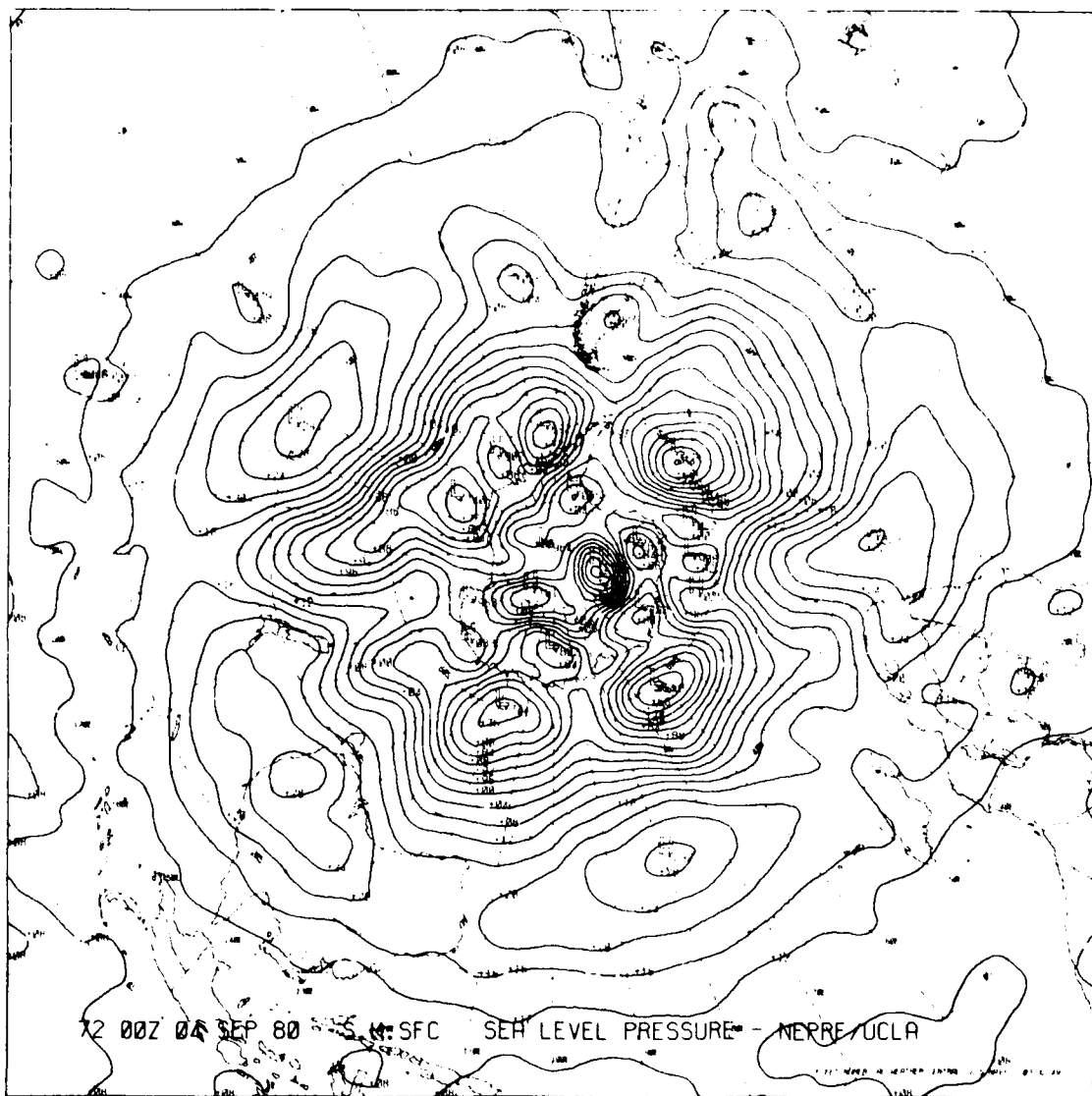


Fig. 2f — 72 hr. sea level pressure (mb), Southern Hemisphere, with MSES

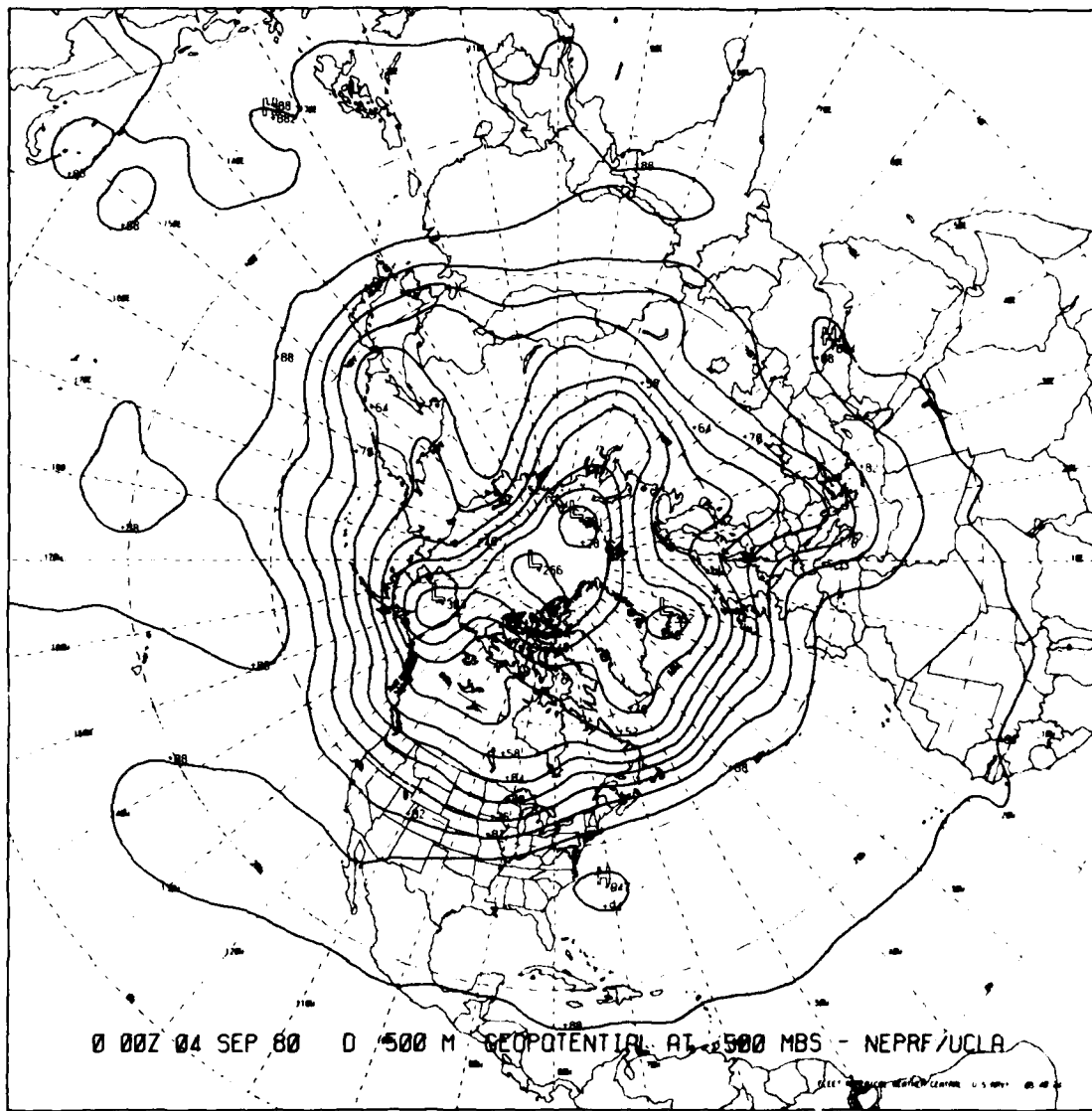


Fig. 3a — Initial 500 mb geopotential (60 meter interval), Northern Hemisphere

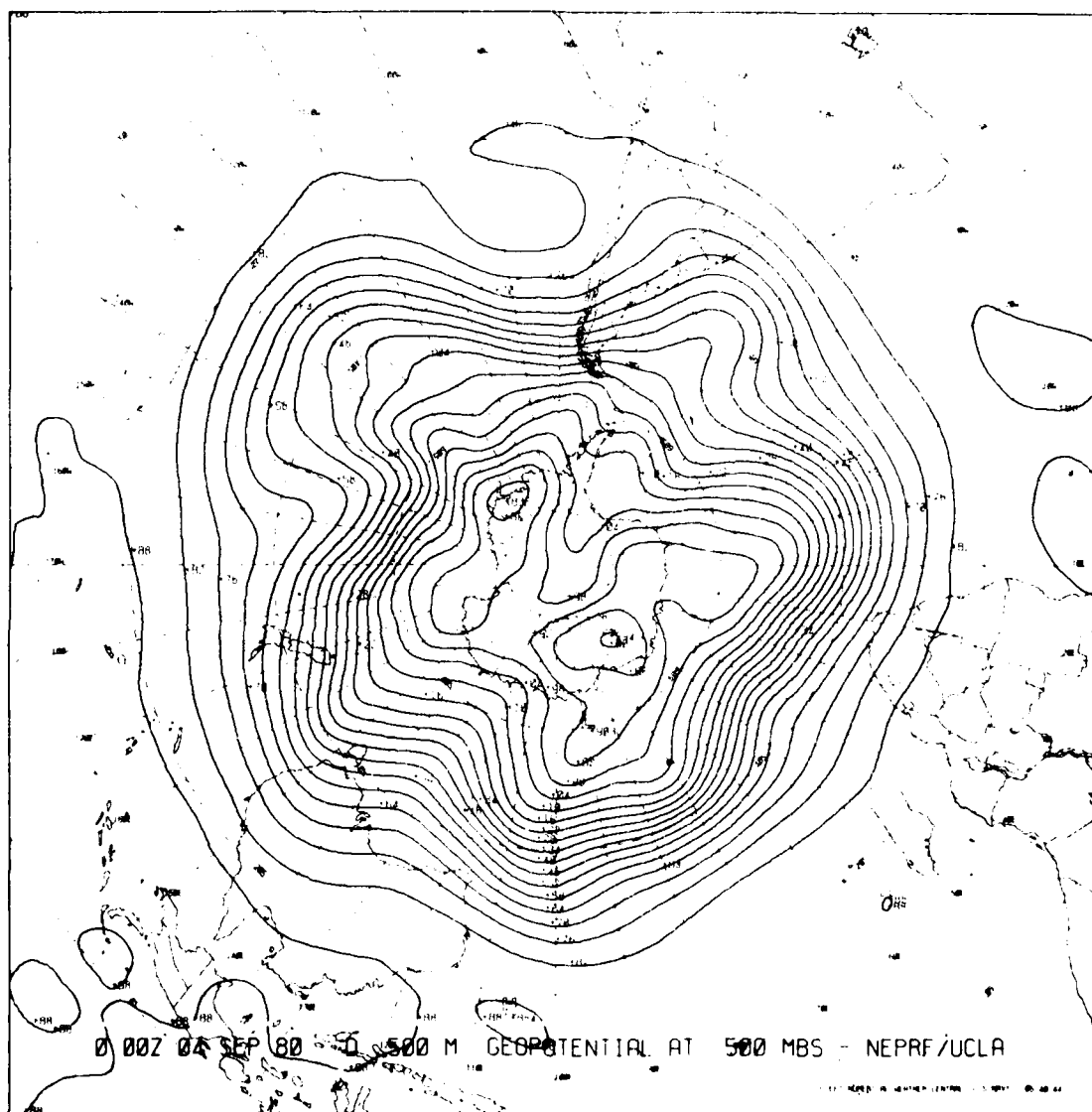


Fig. 3b — Initial 500 mb geopotential (60 meter interval), Southern Hemisphere

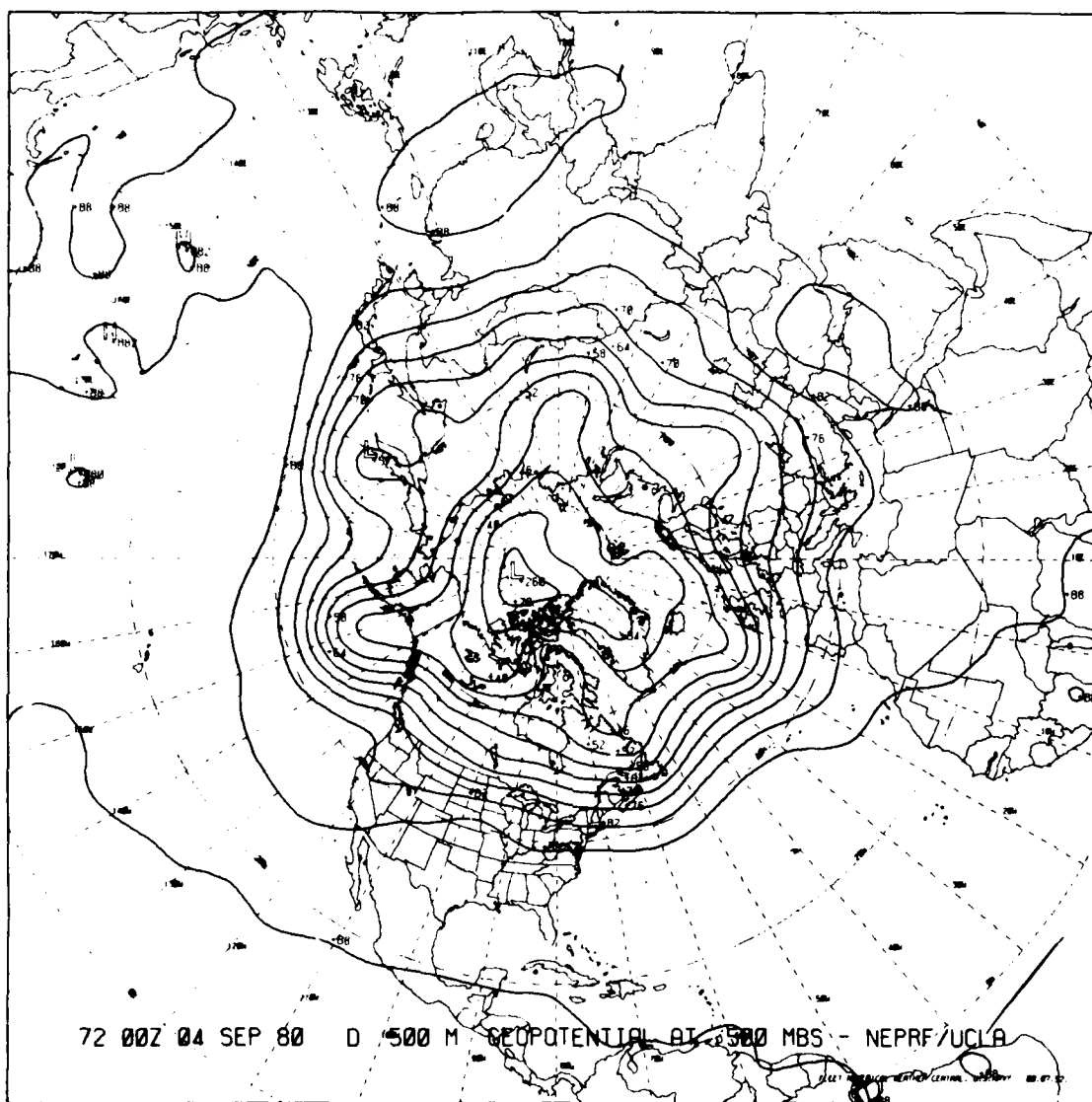


Fig. 3c — 72 hr. 500 mb geopotential (60 meter interval), Northern Hemisphere, no MSES

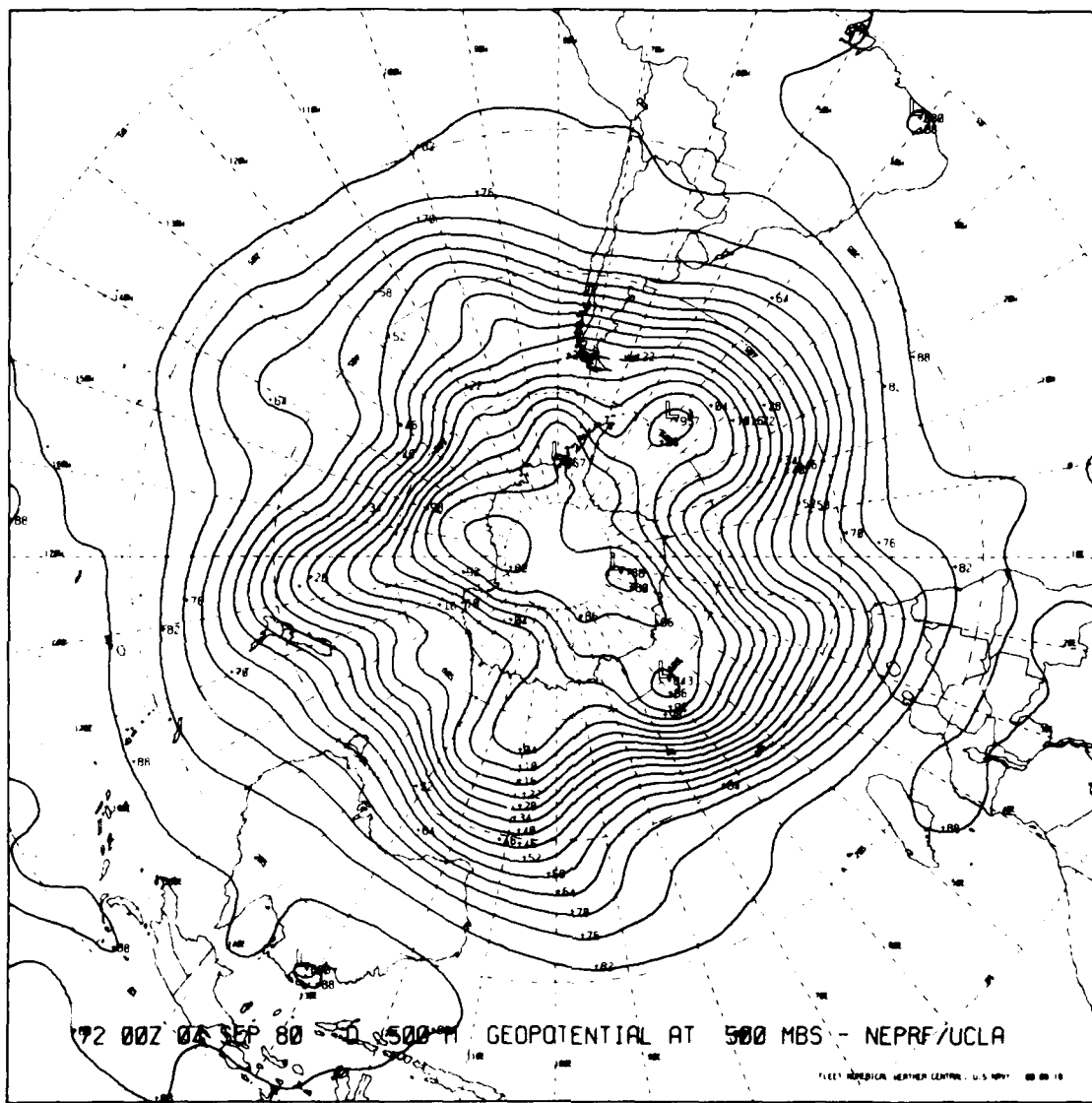


Fig. 3d - 72 hr. 500 mb geopotential (60 meter interval), Southern Hemisphere, no MSES

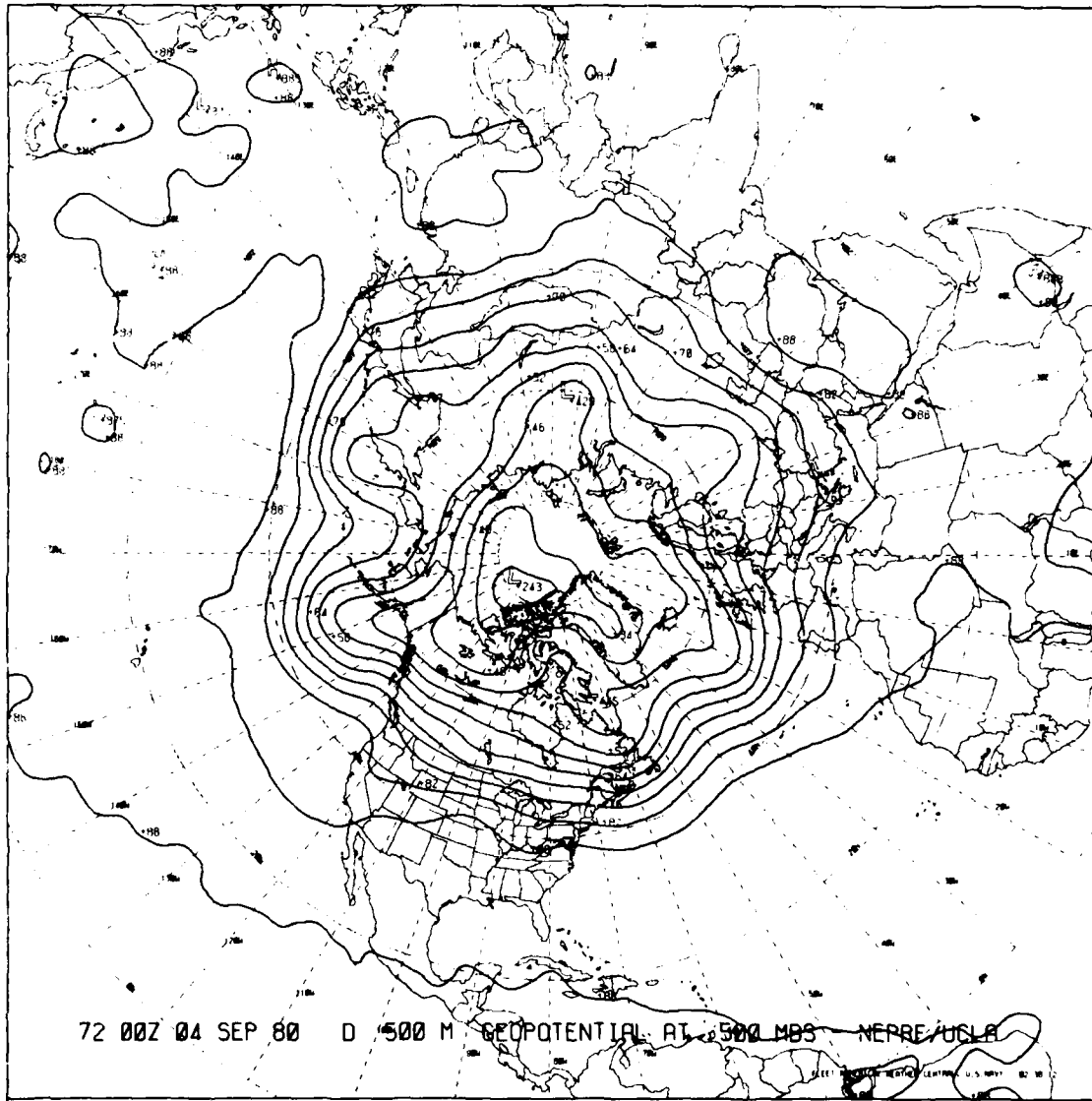


Fig. 3e — 72 hr. 500 mb geopotential (60 meter interval), Northern Hemisphere, with MSES

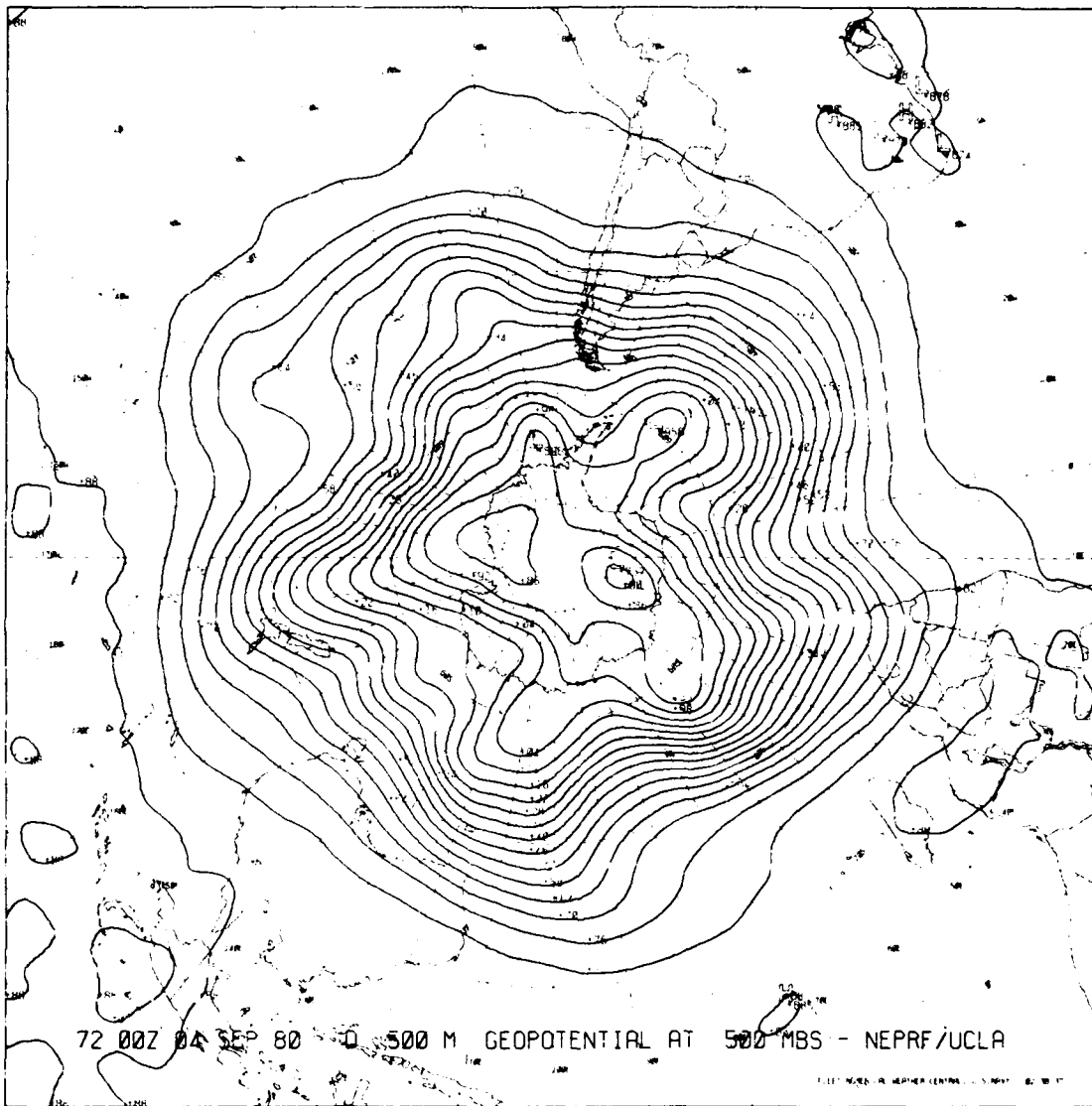


Fig. 3f — 72 hr. 500 mb geopotential (60 meter interval), Southern Hemisphere, with MSES

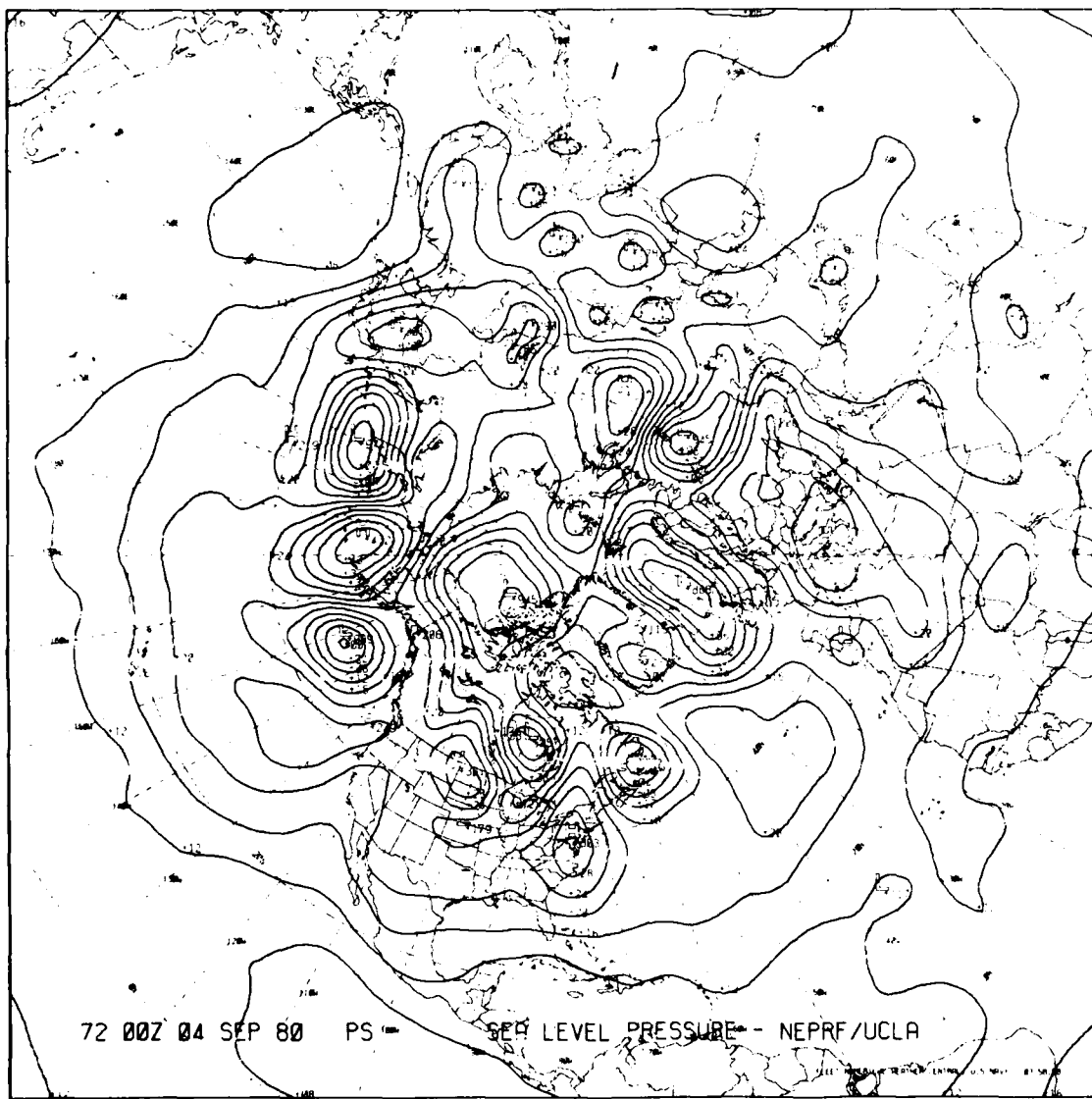


Fig. 4a — 72 hr. sea level pressure (mb), Northern Hemisphere, with MSES, dry model

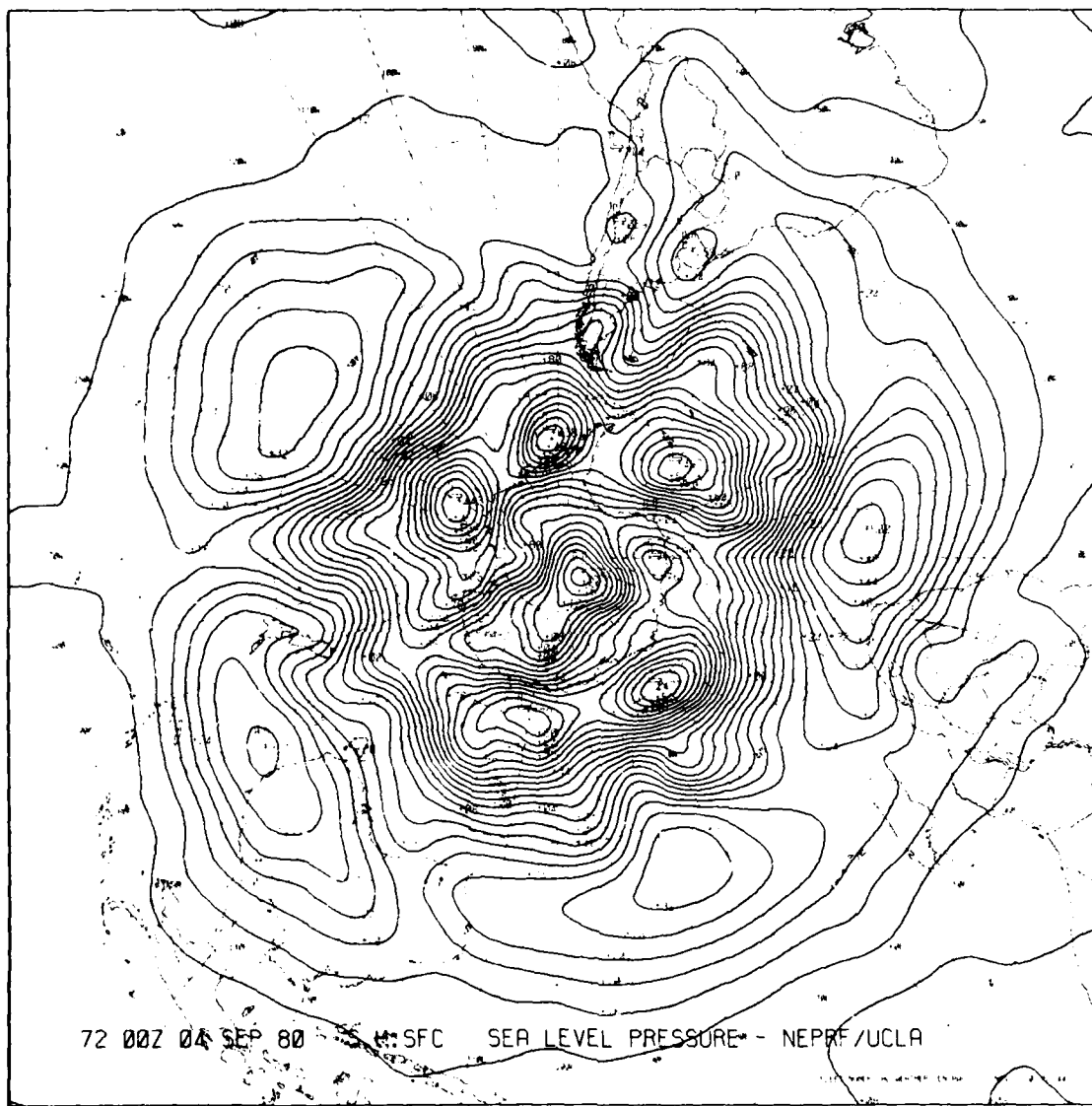
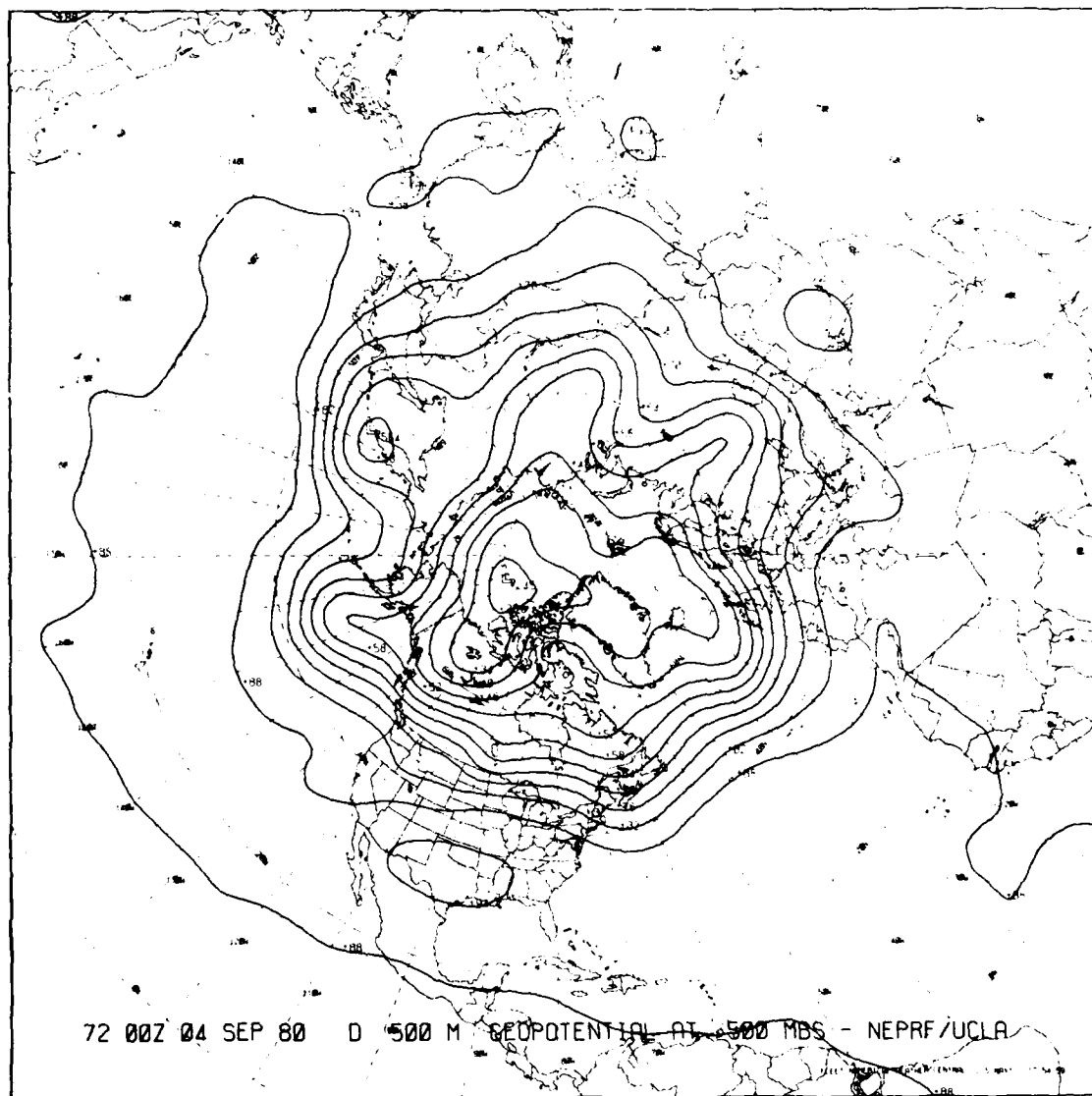


Fig. 4b — 72 hr. sea level pressure (mb), Southern Hemisphere, with MSES, dry model



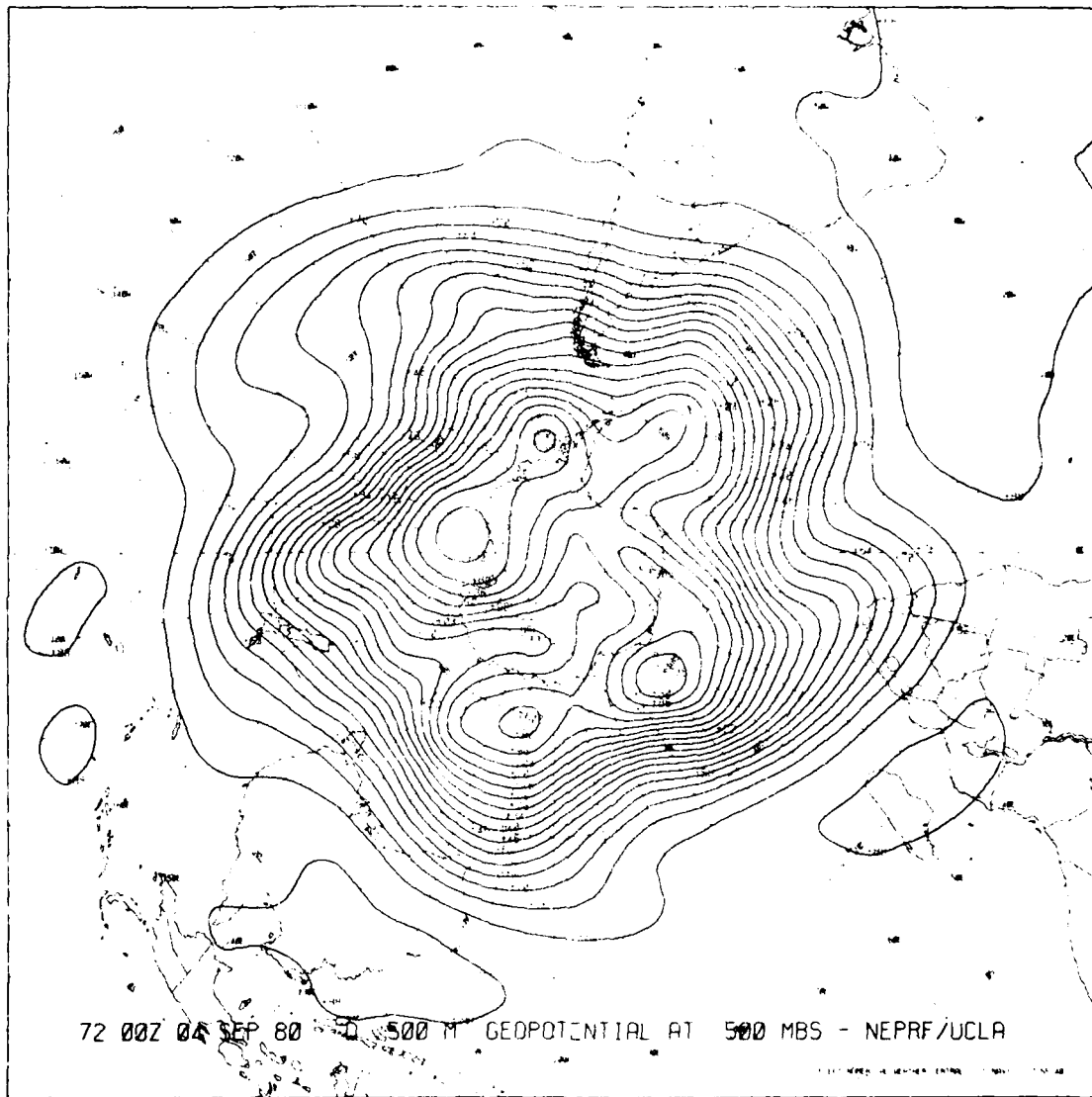


Fig. 4d — 72 hr. 500 mb geopotential (60 meter interval),
Southern Hemisphere, with MSES, dry model

APPENDIX

In a K-level σ coordinate model, where

$$\sigma = (P - P_T) / (P_S - P_T),$$

$$\langle N_2 \rangle^T = (\Delta\sigma_1, \Delta\sigma_2, \dots, \Delta\sigma_K),$$

The hydrostatic equation for ϕ_a (Arakawa, 1972, p. 25) is:

$$(\phi_a)_k - (\phi_a)_{k+1} = \frac{c_p}{2} \left[\left(\frac{T_k}{\bar{p}_{k+1}} \right)^\kappa - \left(\frac{T_{k+1}}{\bar{p}_k} \right)^\kappa \right] \quad (A-1)$$

where $\kappa = R/c_p$, and

$$(\phi_a)_K = \sum_{k=1}^K \bar{\pi}_\sigma \frac{R}{\bar{p}_k} \Delta\sigma_k - (\sigma_{k+1} \beta_k + \sigma_{k-1} \alpha_k) T_k, \quad (A-2)$$

$$\beta_k = \begin{cases} \frac{1}{2} \left[\left(\frac{\bar{p}_{k+1}}{\bar{p}_k} \right)^\kappa - 1 \right] & \text{for } k \leq K-1 \\ 0 & \text{for } k = K, \end{cases}$$

and

$$\alpha_k = \begin{cases} 0 & \text{for } k = 1 \\ \frac{1}{2} \left[1 - \left(\frac{\bar{p}_{k-1}}{\bar{p}_k} \right)^K \right] & \text{for } k \geq 2 \end{cases}$$

The matrix M_1 can be constructed from the preceding equations, where Equations (A-1) and (A-2) give ϕ_k ($k = 1, \dots, K$) as a linear function of T_k ($k = 1, \dots, K$). The element $(M_1)_{i,j}$ equals the ϕ_i , computed using $T_j = 1$ and $T_k = 0$ for all $k \neq j$.

$$[N_1] = - \begin{pmatrix} \Delta\sigma_1 & 0 & \dots & 0 \\ \Delta\sigma_1 & \Delta\sigma_2 & \dots & 0 \\ \dots & \dots & \dots & \dots \\ \Delta\sigma_1 & \Delta\sigma_2 & \dots & \Delta\sigma_K \end{pmatrix} + \begin{pmatrix} \sigma_2^E \Delta\sigma_1 & \sigma_2^E \Delta\sigma_2 & \dots & \sigma_2^E \Delta\sigma_K \\ \sigma_3^E \Delta\sigma_1 & \sigma_3^E \Delta\sigma_2 & \dots & \sigma_3^E \Delta\sigma_K \\ \dots & \dots & \dots & \dots \\ \sigma_{K+1}^E \Delta\sigma_1 & \sigma_{K+1}^E \Delta\sigma_2 & \dots & \sigma_{K+1}^E \Delta\sigma_K \end{pmatrix} \quad (A-3)$$

σ^E denotes σ at an interface between two layers as shown in Fig. A-1. When $\langle \pi \dot{\sigma} \rangle = [N_1] \langle D \rangle$ is substituted in the thermodynamic equation M_2 and M_4 can easily be constructed.

The thermodynamic equation is

$$\begin{aligned} \frac{\partial}{\partial t} (\pi T_k) + \pi \cdot (v_k T_k) + \frac{1}{\Delta\sigma_k} (\kappa \dot{\sigma})_{k+\frac{1}{2}} p_k \hat{\theta}_{k+\frac{1}{2}} \\ - (\pi \dot{\sigma})_{k-\frac{1}{2}} p_k \hat{\theta}_{k-\frac{1}{2}} \end{aligned} \quad (A-4)$$

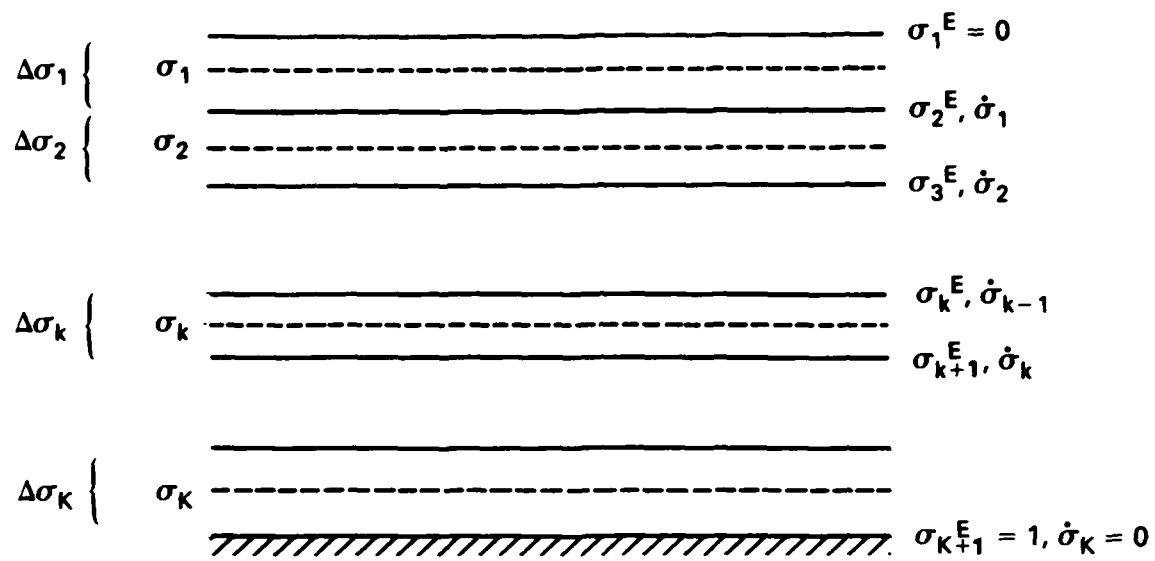


Fig. A1 — Schematic diagram indicating the definitions of σ , σ^E and $\Delta\sigma$

$$= \underbrace{\pi \frac{T_k}{P_k} \frac{\partial P_k}{\partial \pi}}_{||} \left(\frac{\partial}{\partial t} + v_k \cdot \nabla \right) \pi + \pi Q_k / c_p,$$

$$\frac{1}{c_p} (\sigma \pi \alpha)_k$$

where $\hat{\theta}_{k+\frac{1}{2}} = \frac{\ln \theta_k - \ln \theta_{k+1}}{\frac{1}{\theta_{k+1}} - \frac{1}{\theta_k}},$

Thus,

$$\frac{\partial}{\partial t} \langle \pi T \rangle + [T] \langle D \rangle + [M_4] \langle D \rangle = - \langle \frac{\sigma \pi \alpha}{c_p} \rangle \langle N_2 \rangle^T \langle D \rangle + \langle R \rangle_T,$$

where

$$[T] = \begin{pmatrix} \bar{\bar{T}}_1 & 0 & \text{---} & 0 \\ 0 & \bar{\bar{T}}_2 & \text{---} & \text{---} \\ \text{---} & \text{---} & \text{---} & \text{---} \\ 0 & \text{---} & \text{---} & \bar{\bar{T}}_K \end{pmatrix}$$

and

$$[M_4]_{k,j} = (v_{k,j} p_k \hat{\theta}_{k+\frac{1}{2}} - v_{k-1,j} p_k \hat{\theta}_{k-\frac{1}{2}}) / \Delta \sigma_k,$$

where $V \equiv [N_1]$

and

$$[M_2] = [M_4] + [T] + \frac{1}{c_p} \begin{pmatrix} (\sigma\pi\alpha)_1 \langle N_2 \rangle^T \\ \vdots \\ \vdots \end{pmatrix}.$$

It should be emphasized here that all quantities in the matrices are computed using the globally averaged temperature and surface pressure.

REFERENCES

- Arakawa, A., 1972: Design of the UCLA general circulation model. Numerical Simulation of Weather and Climate, Dept. of Meteorology, Univ. of California, Los Angeles, Tech. Report. 7, 116 pp.
- Arakawa, A., and Lamb, V. R., 1977: Computational design of the UCLA General Circulation Model. Methods in Computational Physics, Vol. 17, Academic Press, 173-265.
- Arakawa, A., and Mintz, Y., 1974: The UCLA atmospheric general circulation model, Workshop notes, Dept. of Meteorology, UCLA.
- Brown, J. A., and Campana, K., 1978: An economical time-differencing system for numerical weather prediction, Mon. Wea. Rev. 106, 1125-1136.
- Burridge, D. M., 1975: A split semi-implicit reformulation of the Bushby-Timpson 10-level model, Quart. J. R. Met. Soc., 101, 777-792.
- Courant, R., Friedrichs, K., and Lewy, H., 1928. Über die partiellen Differenzengleichungen der mathematischen Physik. Math. Annalen, 100, 32-74.
- Gadd, A. J., 1978: A split explicit integration scheme for numerical weather prediction, Quart. J. R. Met. Soc., 104, 569-582.

- Kwizak, M., and Robert, A. J., 1971: A semi-implicit scheme for grid point atmospheric models of the primitive equations. Mon. Wea. Rev., 99, 32-36.
- Madala, R. V., 1981: Efficient time integration schemes for atmosphere and ocean models, Chap. 4, Finite-difference techniques for vectorized fluid dynamics calculations, Springer Series in Computational Physics.
- Marchuk, G. I., 1974: Numerical methods in weather prediction. Academic Press, 277 pp.
- Messinger, F., and Arakawa, A., 1976: Numerical methods used in atmospheric models. WMO-ICSU GARP Publication Series No. 17, 64 pp.
- Robert, A. J., 1969 : The integration of a spectral model of the atmosphere by the implicit method. Proc. WMO/IUGG Symposium on Numerical Weather Prediction in Tokyo, 1968. Meteor. Soc. Japan. VII-19-VII-24.
- Robert, A. J., Henderson, J., and Turnbull, C. A., 1972: An implicit time integration scheme for baroclinic models of the atmosphere. Mon. Wea. Rev., 100, 329-335.
- Shuman, F. G., 1971: Resuscitation of an integration procedure. NMC Office Note 54, 55 pp.

DISTRIBUTION LIST

Chief of Naval Research
800 North Quincy Street
Arlington, VA 22217
ATTN: Code 465
Code 460

Chief of Naval Operations (OP-986G)
Navy Department
Washington, D.C. 20350

Chief of Naval Material (MAT-034)
Navy Department
Washington, D.C. 20360

Director
Naval Research Laboratory
Washington, D.C. 20375
ATTN: Code 4700, T. Coffey 25 copies of open publication
1 copy if otherwise
Code 4780, S. Ossakow 150 copies if open publication
1 copy if otherwise

Director
Office of Naval Research
Branch Office
495 Summer Street
Boston, Mass. 02210

Dr. Robert E. Stevenson
Office of Naval Research
Scripps Institution of Oceanography
LaJolla, CA 92037

Chairman
Naval Academy
Environmental Sciences Department
Annapolis, MD 21402

Dr. G. J. Haltiner
Department of Meteorology
Naval Postgraduate School
Monterey, CA 93940

Dr. Dale Leipper
Department of Oceanography
Naval Postgraduate School
Monterey, CA 93940

Naval Air Systems Command (AIR-370)
Washington, D. C. 20361

Naval Air Systems Command (AIR-OSF)
Washington, D.C. 20361

Naval Weapons Center
Code 602
China Lake, CA 93555

Naval Ocean Systems Center
Code 2220
San Diego, CA 92152

Commanding Officer
Naval Ocean R&D Act.
N.S.T.L. Station, MS 39529

Commanding Officer
Fleet Numerical Weather Central
Monterey, CA 93940

Commanding Officer
Naval Environment Prediction Research Facility
Monterey, CA 93940

Commander
Air Force Geophysics Laboratory
Bedford, MA 01730
ATTN: Dr. A. I. Weinstein

Commander
Air Weather Service
Scott AFB, ILL 52225
ATTN: LCOL R. Lininger

Office of the Chief of Research & Development
Department of the Army
Washington, D.C. 20301
ATTN: Environmental Sciences Division

Military Assistant
Environmental Sciences
OSD/ODDRE
Washington, D.C. 20301

Atmospheric Sciences Section
National Science Foundation
1800 G Street, N.W.
Washington, D.C. 20520

National Center for Atmospheric Research
Library Acquisitions
P. O. Box 1470
Boulder, CO 80302

Laboratory of Atmospheric Physics
Desert Research Institute
University of Nevada
Reno, Nevada 89507
ATTN: Dr. Patrick Squires

Carlspan Corporation
P. O. Box 235
Buffalo, NY 14221
ATTN: Mr. Roland Pilie

NORPAX
Scripps Institute of Oceanography
LaJolla, CA 92037
ATTN: Mr. Robert Peloquin

Geophysics Division
Pacific Missile Range
Pt. Mugu, CA 93042
ATTN: CDR. D. B. Pickenscher

Office of Naval Research
Pasadena Branch Office
1030 East Green Street
Pasadena, CA 91105
ATTN: Mr. Ben Cagle

Director
Naval Research Laboratory
Washington, D.C. 20375
ATTN: Code 8320

Defense Documentation Center 12 copies
Cameron Street
Alexandria, VA 22314

Naval Research Laboratory 20 copies
Washington, D.C. 20375
ATTN: Code 2628